# Formation of secondary organic aerosol in the Paris pollution plume and its impact on surrounding regions

Q. J. Zhang[1, 4], M. Beekmann [1], E. Freney [2], K. Sellegri [2], J.M. Pichon [2], A. Schwarzenboeck [2], A. Colomb [2], T. Bourrianne [3], V. Michoud [1,5], A. Borbon [1]

[1] Laboratoire Interuniversitaire des Systèmes Atmosphériques (LISA/IPSL), UMR CNRS 7583, Université Paris Est Créteil (UPEC) and Université Paris Diderot (UPD), France

[2] Laboratoire de Météorologie Physique, Clermont-Ferrand, France

[3] Centre National de Recherches Météorologiques, Météo-France, Toulouse, URA1357, France

[4] Now at Aria Technologies, Boulogne-Billancourt, France

[5] Now at Mines Douai, SAGE, F-59508, Douai, France

**Abstract:** Secondary pollutants such as ozone, secondary inorganic aerosol, and secondary organic aerosol formed in the plume of megacities can affect regional air quality. In the framework of the FP7 / EU MEGAPOLI project, an intensive campaign was launched in the Greater Paris Region in July, 2009. The major objective was to quantify different sources of organic aerosol (OA) within a megacity and in its plume. In this study, we use airborne measurements aboard the French ATR-42 aircraft to evaluate the regional chemistry-transport model CHIMERE within and downwind the Paris region. Two mechanisms of secondary OA (SOA) formation are used, both including SOA formation from oxidation and chemical aging of primary semi-volatile and intermediate volatile VOCs (SI-SOA) in the volatility basis (VBS) framework. As for SOA formed from traditional VOC precursors (traditional SOA), one applied chemical aging in the VBS framework adopting different SOA yields for high and low $NO_x$ environments, while another applies a single step oxidation scheme without chemical aging. Two emission inventories are used for discussion of emission uncertainties. Slopes of the airborne OA levels versus $O_x$ ($=O_3+NO_2$) show SOA formation normalized with respect to photochemical activity and are used for specific evaluation of the OA scheme in the model. Simulated slopes overestimated slightly by a factor of 1.1, 1.7 and 1.3 with respect to the observed one for the three airborne measurements, when the most realistic "high-$NO_x$" yields for traditional SOA formation in the VBS scheme are used in the model. In addition, these slopes are relatively stable from one day to another, which suggests that they are characteristic for the given megacity plume environment. The configuration with increased POA emissions, and with a single step oxidation scheme of traditional SOA gives also agreement with $OA/O_x$ slopes (about ±50% with respect to the observed ones), however, it underestimates the background. Both configurations are coherent with observed OA plume build-up, but they show very different SI-SOA and traditional anthropogenic SOA (ASOA)

contributions. It is hence concluded that available theoretical knowledge and available data in this study are not sufficient to discern the relative contributions of different types of anthropogenic SOA in the Paris pollution plume, while its sum is correctly simulated. Based on these simulations, for specific plumes, the anthropogenic OA build-up can reach between 8 and 10 µg $m^{-3}$. For the average of the month of July 2009, maximum OA increases due to emissions from the Paris agglomeration are noticed close to the agglomeration at various length scales: several tens (for primary OA) to hundred (for SI-SOA and ASOA) kilometers of distance from the Paris agglomeration. Also BSOA (SOA formed from biogenic VOC precursors) is an important contributor to regional OA levels (inside and outside the Paris plume).

## 1. Introduction

The number of large agglomerations ("megacities") is increasing due to population clustering in urban regions (UN, 2011). Human activities in the megacities cause important negative effects on air quality (Gurjar et al., 2010). Pollutants like ozone and fine particulate matter ($PM_{2.5}$) have recently been the focus of several studies as a result of concerns for human health, impact on ecosystem (Seinfeld and Pandis, 2006) and climate (IPCC, 2013). Due to their life time (several days to weeks), $PM_{2.5}$ and ozone have impacts at both the local and regional level. Therefore, adequate emission control strategies for air quality management need to take into account impacts on different scales.

Photochemical ozone formation is related to precursor molecules: nitrogen oxides ($NO_x$), and volatile organic compounds species (VOC), emitted mainly from human activities, such as traffic, industrial production, solvent use, but also from biogenic emissions. In large European agglomerations, a VOC limited chemical regime is in general realized (Beekmann and Vautard, 2010), in which ozone production is directly related to that of VOC precursors. Secondary aerosol formation is induced by formation of condensable or semi-volatile species from precursors like $NO_x$, $SO_2$, $NH_3$ and VOC (Seinfeld and Pandis, 2006). Due to the large number of chemical reactions occurring in different phases, secondary organic aerosol (SOA) formation pathways are still uncertain (e.g. Hallquist et al., 2009), its formation is still difficult to estimate quantitatively (e.g. Hodzic et al., 2010, Zhang et al., 2013), and the contribution of anthropogenic versus biogenic sources are still under debate (e.g. Hallquist et al., 2009, Beekmann et al., 2015). Also the relative contribution of SOA from traditional anthropogenic VOC precursors (ASOA) and from semivolatile (SVOC) or intermediate

volatility (IVOC) organic compounds (SI-SOA) is still under debate and difficult to constrain from field data (as for example discussed in Hayes et al. 2015 for the case of Los Angeles).

Field data provide strong constraints on SOA related processes. In particular, the relation between SOA and $O_x$ ($O_3$ + $NO_2$) has been used to express SOA formation as a function of photochemical products formation (Herndon et al., 2008, Wood et al., 2010; Hayes et al. 2013; Morino et al. 2014). Indeed, in a "VOC-limited regime" in an urban area, such as Paris, VOC oxidation by OH, ozone or $NO_3$ is the rate limiting step for both SOA and ozone or $O_x$ production.

(1) $$VOC + OH \rightarrow \cdots \rightarrow \cdots \rightarrow \alpha\, O_x + \beta\, SOA + \cdots$$

The ratio or slope of SOA vs. $O_x$, given by the term $\beta/\alpha$ represents the ratio of the photochemical production of SOA to the photochemical production of $O_x$, both from VOC oxidation, that is, the SOA yield normalized by current photochemical conditions characterized by the availability of VOC precursors and oxidant agents. It is expected to vary for different VOC species, in particular as a function of their SOA yields, which are for instance large for aromatics and terpenes, while low for alkanes and alkenes (Wood et al., 2010). This is reflected in larger SOA vs. $O_x$ slopes observed in Mexico City (typically 0.16 µg $m^{-3}$ $ppb^{-1}$), in Los Angeles (0.15 µg $m^{-3}$ $ppb^{-1}$, Hayes et al. 2013) and in Tokyo (0.19 µg $m^{-3}$ $ppb^{-1}$, Morino et al. 2014), where aromatic emissions are large, than in Houston (typically 0.03 µg $m^{-3}$ $ppb^{-1}$) where petrochemical alkene emissions are large (Wood et al., 2010) (Fig. 1).

The main objective of the MEGAPOLI Paris campaign in summer 2009 was to determine organic aerosol sources in a post-industrial megacity and in its plume. In this work, we apply the regional chemistry transport model (CTM) CHIMERE (Menut et al., 2013) in order to evaluate the model performance against airborne measurements especially for organic aerosol and to assess the impact of Paris agglomeration emissions on OA formation in surrounding regions.

Different configurations of the SOA formation schemes have been implemented into CHIMERE, in particular the Volatility-Basis-Set (VBS) approach (Robinson et al. 2007, Donahue et al. 2006, Murphy and Pandis, 2009, Lane et al. 2008a). Based on ground level evaluation with data from the MEGAPOLI summer campaign, Zhang et al. (2013) show a better agreement with OA measurements, when taking into account the volatility of primary organic aerosol (POA), the existence of additional intermediate VOC (IVOC), as well as the chemical aging of the semi-volatile VOC from anthropogenic and biogenic origin. However,

SOA was overestimated during long range transport episodes of polluted plumes to the Paris agglomeration. In addition, also uncertainties of POA (or SI-VOCs) emissions were made evident and estimated at least at a factor of three (Zhang et al. 2013).

For megacities, sources of organic aerosol are still under debate and need to be quantified (e.g. Molina et al., 2010). While in Beekmann et al. (2015), the local versus advected and the fossil versus non fossil nature of OA sources within the agglomeration is analyzed, here we focus on additional OA build-up in the agglomeration plume, and on its impact on aerosol concentrations in the surrounding of Paris. In the framework of the MEGAPOLI project, airborne measurements were performed with the French ATR-42 aircraft operated by the SAFIRE (a CNRS-MétéoFrance–CNES headed unit) in order to document the evolution of pollutants within the Paris agglomeration pollution plume during the MEGAPOLI summer campaign (Freney et al., 2014). The advantage of the airborne measurements over the ground based ones is to follow the evolution of the city plume over time and space up to 200 km downwind of the emissions. Data from these flights will be used to extend the model evaluation performed in Zhang et al. (2013) for urban and suburban sites in the Paris agglomeration to plume conditions. Focus is to monitor the build-up of secondary organic aerosol within the plume in relation with tracers of primary emissions, and photochemical activity. Among the various formulations that have been derived in the framework of the VBS scheme (for example, Lane et al., 2008, Murphy and Pandis., 2009, Dzepina et al., 2011, Shrivastava et al., 2013, Zhao et al., 2015, etc.), specifically two are chosen for this paper (as already for Zhang et al., 2013), because they either favor large ASOA or large SI-SOA build-up in the plume. In this way, we intend to address uncertainty linked to the co-existence of different VBS schemes in the formation of different SOA types within the plume. Another important aspect of this paper is to analyze the $OA/O_x$ ratio, specifically used for model evaluation, as it normalizes SOA formation with respect to photochemical reactivity and precursor load.

The paper is organized as follows. In section 2, the airborne measurements during the MEGAPOLI summer campaign are described. The model configurations and simulation set-ups for the VBS approach to model POA and SOA are introduced in section 3. The evaluation of model performance for plume simulations is presented in section 4, and the impact on regional air quality is described in section 5. From comparison of different set-ups of the VBS scheme, uncertainties in the formation of different SOA types in the Paris plume are discussed.

## 2. Airborne measurement during the MEGAPOLI summer campaign

Flight patterns flown during the MEGAPOLI campaign (Fig. 2) consisted of several transects of the pollution plume at increasing distances from the urban area (Freney et al., 2014). Perpendicular flight legs to the plume axis were chosen ranging from 50 to 100 km in order to sample both the plume and rural background conditions at the lateral plume edges. Taking into account the aircraft autonomy of about 3.5 hours, this allowed flying four legs across the plume. The maximal distance for a flight was about 200 km from the Paris agglomeration center. The flight level was chosen to lie well inside of the well-developed afternoon convective boundary layer, at about 500-700 m above ground. In addition to measurements inside and outside the Paris plume, each flight included a complete circle around the agglomeration, performed after starting and before landing at the Cergy-Pontoise airport. In this work, we focus only on measurements downwind of Paris to study the pollution production from Paris emissions. The measurements started in the early afternoon in order to sample photo-chemically processed air. Because of a limited number of flight hours, and in line with the principal objective to document the photochemical production of pollutants, flights were performed on days with light wind (< 3 m $s^{-1}$) and cloud free weather conditions. For this study, three flights were chosen on the 16$^{th}$, 21$^{st}$ and 29$^{th}$ of July, all of which encountered well pronounced plumes of primary and secondary pollutants. Meteorological conditions for these days were characterized by southerly winds, low wind speed over the agglomeration, elevated temperature and cloudless skies. These conditions favor the accumulation of primary pollutants and photochemical processes leading to the formation of secondary pollutants like $O_3$ and SOA.

An extensive set of gas phase pollutants, aerosol species and properties were measured on each flight (Freney, et al., 2014). For this work, for each flight, a complete measurement set of primary pollutants, BC and $NO_x$ (NO and $NO_2$), and of secondary pollutants, $O_3$ and OA, is available and analyzed. Measurement frequencies of all instruments, including the aerosol chemical composition, are rapid enough (< 40 s) to have a relatively good spatial resolution. All measurements during the flights are corrected to temperature (22 °C) and pressure (950 hPa) of the plane (Freney et al. 2014). Thus compared to other values given in this paper and taken at standard conditions, our values are about 5% lower. Table 1 summarizes the deployed instruments and the measured concentration levels for these pollutants during these flights. Only measurements at a stable flight altitude are used for this study.

The 30$^{th}$ percentile concentration of a pollutant on the flight legs downwind of Paris is close to the median concentration outside the Paris plume and represents its background level. For $NO_x$ and BC, the 30$^{th}$ percentile concentrations are 1.11, 1.03 and 1.14 ppb, and 0.33,

0.49 and 0.38 µg $m^{-3}$ on 16th, 21st and 29th, respectively (Table 1). The rather homogeneous background pollutant levels (Fig. 2 and 3) correspond to the absence of major urban pollution sources on the south of the Paris agglomeration (rural "Centre" region). The Paris pollution plumes are always clearly identifiable as sharp concentration increases, with continuity on all flight legs at different distances from the agglomeration (Fig. 2 and 3). The plume half-widths are about several tens of kilometers. Maximum plume concentrations of $NO_x$ and BC are 13.5, 7.98 and 12.2 ppb, and 2.00, 2.01 and 2.30 µg $m^{-3}$, respectively for the three flights (Table 1).

The maximum plume ozone concentrations are 62.0, 79.0 and 62.4 ppb during these flights, respectively, as compared to the 30th percentile (i.e. background) concentrations of 49.0, 58.0 and 50.0 ppb (Table 1). The largest $O_3$ values are observed at the flight leg most distant from the agglomeration, allowing for the longest photochemical processing (Fig. 4). For the 16th, the transects across the plume show a double maximum and a relative central minimum due to ozone titration by NO.

The background concentrations of OA are 3.87, 6.47 and 4.13 µg $m^{-3}$, respectively during these three flights (Table 1, Fig. 5). Maximum plume OA concentrations are 5.97, 12.33 and 7.36 µg $m^{-3}$, respectively. Thus, additional OA build-up within the plume is about 2 to 6 µg $m^{-3}$ (see also below in section 4.2). Maximum concentrations appear in the three outer flight legs. OA plumes are wider and less homogeneous than primary pollutant ones, which could be due to a secondary organic aerosol production from additional biogenic sources in addition to formation from emissions in the Paris agglomeration.

OA versus $O_x$ ($O_x$=$O_3$+$NO_2$) plots from measurements on these flights are used to study the ratio of the photochemical productivity of OA and $O_x$ build-up in the plume from Paris emissions following an approach first proposed by Herndon et al. (2008). In this study, OA is used instead of SOA, because it is directly measured. Among OA factors derived from Positive Matrix Factorization (PMF) of AMS measurements, LV-OOA (Low volatility oxygenated) and SV-OOA (Semi volatile oxygenated OA) are commonly attributed to SOA (Hallquist et al., 2009). These LV-OOA and SV-OOA factors contributed on average about 65% of resolved OA factors and 37% of the total OA during these three MEGAPOLI flights. HOA (hydrocarbon like OA) make up for the remaining 35% of resolved OA factors and 20% of the total OA. While the HOA factor is generally attributed to POA, it might partly also correspond to oxidized POA, considered as SOA (Aumont et al., 2012, Cappa and Wilson, 2012), and to cooking-related OA (Freutel et al. 2013). Using total OA avoids these problems arising from the interpretation of PMF derived factors.

The Pearsons R correlation between OA and $O_x$ on the three flights on 16th, 21st and 29th is around 0.70 (Table 4, Fig. 6). It indicates a similar ratio of photochemical production of ozone and OA from VOC precursors, though as expected the match between OA and $O_x$ is not perfect, due to differences in SOA and $O_x$ yields for different VOC precursors. The $OA/O_x$ slopes for these flights are 0.14-0.15 µg $m^{-3}$ $ppb^{-1}$. This result is close to the one obtained from a previous flight study of urban air mass in Mexico City (0.14-0.15 µg $m^{-3}$ $ppb^{-1}$, Wood et al., 2010). It is also close to ground-based study, downwind urban emissions from ground-based measurements in Mexico City (median OOA vs. $O_x$ slope of 0.16 µg $m^{-3}$ $ppb^{-1}$, Wood et al., 2010), in Los Angeles (0.15 µg $m^{-3}$ $ppb^{-1}$, Hayes et al. 2013) and in Tokyo (0.19 µg $m^{-3}$ $ppb^{-1}$, Morino et al., 2014).

## 3. Simulations

### 3.1 Model Configuration

In this work, we used the CHIMERE v2008b model (see http://www.lmd.polytechnique.fr/chimere/) (Vautard al. 2001, Bessagnet et al. 2009, Menut et al., 2013), widely used for operational regional air quality forecast (Honoré et al, 2008, Zhang et al. 2012) and simulations in Europe (e.g. Beekmann and Vautard, 2010, Sciare et al, 2010). With a few exceptions (noted below), the same model configuration as in Zhang et al. (2013) was set-up. Two nested domains are applied: a continental domain covering Europe with a resolution of 0.5° (35–57.5°N, 10.5°W–22.5°E) and a regional domain over Northern France covering all the flight patterns during this campaign with a resolution of 3 km (called MEG3 domain). 8 hybrid-sigma vertical layers are used, with the first layer extending from ground to about 40 m, and a model top at 500 hPa. Tropospheric photochemistry is represented using the reduced MELCHIOR chemical mechanism (Lattuati, 1997, Derognat et al., 2003), including 120 reactions and 44 prognostic gaseous species. For the simulation of the particulate phase, 8 bins of particulate sizes are used in the model with diameters ranging from 0.04 to 10 micrometers. The thermodynamic equilibrium of the inorganic species (sulfate, nitrate, and ammonium) between the gas and particle phase is interpolated from a tabulation calculated with the ISORROPIA model (Nenes et al., 1998). The evaporation and condensation processes related to departures from the thermodynamic equilibrium are kinetically controlled.

Two SOA formation mechanisms are used and are described in more detail in section 3.2. For SI-SOA (SOA from oxidation of primary semi-volatile and intermediate volatile VOCs, previously referred to as OPOA in Zhang et al. 2013) formation, both mechanisms use

the VBS formulation as described in Robinson et al. (2007). For traditional anthropogenic and biogenic SOA (ASOA and BSOA) formation from VOC precursors, one uses the classical single step oxidation scheme (Pun et al. 2006, Bessagnet et al., 2009), and the other one a volatility basis set (VBS) scheme with differences in high-$NO_x$ and low-$NO_x$ parametrizations. The VBS approach is implemented in the model as in Murphy and Pandis, (2009) and Lane et al. (2008a). In our work, BSOA gas phase aging is also included with the same rate constant as for ASOA ($1\times10^{-11}$ mol $cm^3$ $s^{-1}$). Gas phase chemical aging of BSOA is supported by laboratory (see in Zhao et al., 2015) and box model experiments with the very detailed GECKO-A mechanism (Valorso et al., 2011). In Zhang et al. (2013), it had been shown that including BSOA aging was necessary to reproduce several OA peaks occurring during the summer campaign at Paris urban sites in the model.

For the large domain, anthropogenic gas phase emissions are calculated from EMEP annual totals (http://www.ceip.at/emission-data-webdab/), while black carbon (BC) and primary organic aerosol (POA) are prescribed from an emissions inventory prepared by Laboratoire d'Aérologie (LA) (Junker and Louisse, 2008). In the different simulation set-up's in section 3.2, emissions for the inner domain MEG3 over Northern France are either taken from the same EMEP-LA inventory, or from an alternative inventory specifically designed for the MEGAPOLI project, the Airparif-TNO-MEGAPOLI inventory, in which the refined Paris emissions from Airparif with a resolution of 1 km are integrated into the European wide TNO inventory (Timmermans et al., 2013). In this latter inventory, BC and POA emissions for the Paris agglomeration are about two and three times lower than in the EMEP-LA inventory, respectively, and VOC emissions are about a third lower, while $NO_x$ emissions are similar. These differences are explained by use of spatial downscaling techniques in the EMEP-LA inventory using proxies that generally tend to overestimate megacity or urban emissions, while the Airparif-TNO-MEGAPOLI inventory is constructed following a bottom-up approach (Timmermans et al., 2013). Both inventories are affected by additional uncertainties in activities and related emission factors. Cooking emissions, which have been shown to be significant for the Paris agglomeration (Freutel et al., 2013, Crippa et al., 2013) are not included in either of these emission inventories. In this work, we assume that differences in BC and POA emissions in both inventories span the range of uncertainty for these emissions for the Paris region. This is compatible with the Petetin et al., (2015) study which evaluates these emission inventories with respect to ground based measurements within the agglomeration and ground based ones around it. As explained in more detail in Zhang et al. (2013), POA/SVOC emission factors for the main source in summer, traffic, are obtained from laboratory measurements under low level of dilution (with OA loading of 1000 µg $m^{-3}$).

Under these conditions, the POA/SVOC emissions are emitted mostly in the particle phase. A volatility distribution following Robinson et al. (2007) was affected to these emissions. Additional IVOC emissions (factor 1.5 of POA/SVOC) were also considered according to Robinson et al. (2007).

Biogenic emissions are calculated using the MEGAN model data and parameterizations (Guenther et al., 2006). Meteorological fields are simulated with the MM5 mesoscale model (Dudhia, 1993). Boundary conditions are taken from a monthly climatology of the LMDz-INCA2 and LMDz-AERO general circulation model (Hauglustaine et al., 2004).

### 3.2 Simulation configurations

Here, a brief summary on the three distinct simulation configurations used in this study is given. They are intended to take into account both uncertainties in SOA formation schemes and in POA/SI-VOC emissions.

- The **VBS-LNOX** simulation, in which all SI-SOA, ASOA and BSOA are affected by chemical aging with the VBS approach. High SOA yields under low-$NO_x$ conditions (Murphy and Pandis, 2009, Lane et al. 2008a) are used for both two simulation domains (the same as the so-called VBS-MPOLI simulation in Zhang et al., 2013, see Table 2), assuming that most of OA is advected to the Paris agglomeration from outside (Petetin et al., 2014) and probably formed under low-$NO_x$ conditions. Usually, a limiting VOC/$NO_x$ ratio of 3 and 10 ppbC $ppb^{-1}$ is used to discern a high and a low $NO_x$ regime, respectively (Lane et al., 2008b). While the ratio of 10 ppbC $ppb^{-1}$ is close or above the value for most of Northern France, indicating that it is close to a low-$NO_x$ regime, it is close to or below the ratio of 3 ppbC $ppb^{-1}$ on the north of Paris in the plume region (Fig. S1). This low-$NO_x$ configuration is thus expected to overestimate ASOA formation in the Paris pollution plume under high $NO_x$ conditions around Paris. The emission inventory for the MEG3 domain is the specific MEGAPOLI inventory.

- The **VBS–HNOX** simulation in which lower SOA yields under high-$NO_x$ conditions (Murphy and Pandis, 2009, Lane et al. 2008a) are used for the inner MEG3 domain (see Table 2). This is more realistic for SOA formation in its plume close to the Paris agglomeration than low $NO_x$ condition. The low-$NO_x$ condition is still applied on the continental domain for background OA simulation. All other model settings are equal

to the VBS-LNOX configuration. Although using high-$NO_x$ conditions with lower yields, which are more realistic for the plumes from Paris emissions, this configuration might still overestimate ASOA formation in the plume following the new ASOA yields fitted to laboratory experiments in SOA formation schemes described in Zhao et al. (2015).

- The **VBS-LA** simulation (same as VBS-T1 simulation in Zhang et al., 2013) in which a single step oxidation scheme (Pun et al. 2006) is used for traditional ASOA and BSOA formation, and the VBS scheme for SI-SOA formation as for the other two configurations. The EMEP-LA emission inventory with three times larger POA/SI-VOC emissions is used for the inner MEG3 domain. The fact that POA/SI-VOC emissions are three times larger and the absence of chemical aging for ASOA will favor SI-SOA with respect to ASOA formation.

## 4. Model evaluation with airborne measurements

In this section, modeling results of $NO_x$, BC, $O_x$, and OA are presented and compared to the airborne measurements at the same location and time. Outputs from simulations are interpolated to the exact flight location and time. $NO_x$ and BC are compared as primary urban tracers to indicate the location of the Paris plume in observations and in simulations. Only the VBS-LNOX simulations are used for BC, $NO_x$ and $O_x$, because a change of the SOA yields does not affect the simulation of the concentrations of these species between the VBS-LNOX and VBS-HNOX simulations. The evaluation with the VBS-LA simulations gives an insight on effects of emission uncertainties. Individual species comparisons are presented in section 4.1 while model observation comparisons of the $OA/O_x$ ratio are presented in section 4.2. For each of the 4 to 5 transects through the pollution plume of a flight, the simulated and observed maximum concentrations are depicted and averaged over all transects of a flight. The same procedure is applied for $30^{th}$ percentiles (P30) over each transect, considered as representative for background conditions outside of the plume.

### 4.1 Individual species model to observation comparisons

The qualitative inspection of simulated and observed BC plumes shows that the plume direction is correctly simulated on the $21^{st}$ and $29^{th}$, while a difference of about 20° occurs on $16^{th}$ (Fig. 2). This will have little influence on the study on OA impact from Paris to its

surroundings due to the rather circular structure of the agglomeration (Shaiganfar et al., 2015). In both the modeled fields and in the observations, the largest concentrations appear close to the Paris agglomeration during these three flights.

The modeled maximum BC concentrations from VBS-LNOX are underestimated by -0.7 (-35%), -1.5 (-74%) and -1.6 µg $m^{-3}$ (-70%) with respect to the measurement, respectively for the 16$^{th}$, 21$^{st}$, and 29$^{th}$, while they are overestimated by 0.4 (21%) and underestimated by -1.2 (-62%) and -1.2 µg $m^{-3}$ (-53%) from VBS-LA, respectively (Table 3 and S1, Fig. 2). Thus for the last two flights, the BC underestimation appears for both emission inventories. An average underestimation of plume BC measurements by –20% (over 10 flights during July 2009) was already noticed by Petetin et al. (2015). It could be attributed to errors in emission inventories, uncertainty in measurements and in the choice of the mass specific absorption coefficient (Petetin et al., 2015). Our study focusses on three days with particularly low wind speeds with variable wind direction during morning hours in the Paris agglomeration, allowing for primary pollution build-up and subsequent secondary pollution build-up in the plume. As shown in Petetin et al. (2015), it turns out that the meteorological model (MM5, but similar results are obtained for WRF) forcing the CTM simulations is not capable of simulating these wind direction variations for two of the three flight days, on 21$^{st}$ and 29$^{th}$ of July, thus underestimating the pollution accumulation in the Paris region, and subsequently in the plume. The modeled 30$^{th}$ percentile BC concentrations taken as representative for background concentrations are also underestimated by -0.17 (-51%), -0.31 (-62%) and -0.22 µg $m^{-3}$ (-59%) from VBS-LNOX and by -0.22 (67%), -0.34 (-69%) and -0.27 µg $m^{-3}$ (-71%) from VBS-LA, respectively during these flights (Table 3 and S1, Fig. 2).

Similar to BC, VBS-LNOX underestimates $NO_x$ concentrations by -4.3 (-32%), -5.2 (-65%) and -7.3 ppb (-60%) for the maximum concentrations and by -0.64 (-58%), -0.42 (-41%) and -0.59 ppb (-52%) for the background concentrations with respect to the measurements (Table 3 and S1, Fig. 3). VBS-LA shows slightly more underestimation by -7.3 (-54%), -5.3(-72%) and -8.7 (-71%) ppb for the maximum concentrations and slightly less underestimated for the background concentrations by -0.57 (-51%), -0.36 (-35%) and -0.51 (56%) ppb (Table 3 and S1). Also similar to BC, the modeled $NO_x$ maximum concentrations for both simulations are located close to the Paris agglomeration (Fig. 2 and 3).

The modeled $O_3$ concentrations are slightly overestimated with respect to the measured $O_3$ concentrations, by 7.5 (12%), 4.3 (5%) and 8.3 ppb (13%) from VBS-LNOX and 12.9 (21%), 4.3 (5%) and 9.8 ppb (16%) from VBS-LA for the maximum concentrations, and 4.3 (9%), 11.3 (20%) and 3.0 ppb (6%) from VBS-LNOX and 4.6 (9%), 11.7 (20%) and

3.3 ppb (7%) from VBS-LA for the background concentrations during the three flights, respectively (Table 3 and S1, Fig. 4). Note that for $O_x$, the concentrations can be slightly less overestimated than $O_3$, by respectively 3.0 (6%), 11.0 (19%) and 1.8 ppb (4%) from VBS-LNOX and 3.4 (7%), 11.4 (19%) and 2.1 ppb (4%) from VBS-LA for the background concentrations due to the opposite sign in measured $O_3$ and $NO_x$ differences (Table 1, 3 and S1, Fig. S2) and sometimes for the maximum concentrations by 8.5 (13%), 3.6 (4%), 8.0 ppb (12%) from VBS-LNOX and 13.1 (21%), 3.5 (4%) and 9.2 ppb (14%) from VBS-LA,. Similar to the observations, the modeled maximum $O_3$ and $O_x$ levels are located at farthest distances from the agglomeration. Differences between VBS-LNOX and VBS-LA are apparently small. The rather correct simulation of $O_3$ and $O_x$ in spite of the $NO_x$ underestimation is less astonishing in light of the following discussion about $NO_x$-OH relationships.

Direct comparisons for POA are not shown here because of the uncertainty in HOA factors from the PMF analysis, and because of the incomplete match between HOA and POA. However, the BC underestimation in simulations lets us also expect a POA underestimation.

Consequences of these underestimations in primary pollutants for the build-up of secondary pollutants are briefly discussed here:

- First, as shown above for BC, the underestimation is alleviated in the alternative VBS-LA simulation with larger BC (and POA) emissions. Thus unexpressed uncertainty in meteorological data is partly taken into account by that in emissions.

- Second, the use of OA vs $O_x$ slopes for evaluation of the SOA production efficiency normalizes out the effect of errors in primary pollutants, as equation (1), it merely depends on the ratio of the product yields. This is why the use of this ratio is important for this study.

- Third, in a VOC limited regime as characteristic for the Paris region (e.g. Deguillaume, et al, 2008), the rate of secondary pollutant build-up is far from proportional to the primary precursor concentration. On the contrary, in the extreme case that $NO_x$ compounds represent the only OH loss, $NO_x$ and OH concentrations are inversely proportional (e. g. Kleinman et al., 1997). When assuming a constant ratio in primary pollutants, the flux in equation (1) is then independent of VOC concentrations, and only depends on the production rate of odd hydrogen radicals ($OH+HO_2+RO_2$).

The measured OA plume is correlated with the measured BC plume on 16th, while it appears translated to the west on 21st and 29th, as is also the ozone plume (Fig. 3, 4 and 5). This is probably due to an additional contribution from other sources besides the Paris emissions, such as background levels from regional contribution related to both anthropogenic and biogenic sources. In the simulations, OA, $O_3$, BC, and $NO_x$ plumes coincide for all dates indicating a contribution from the Paris emissions. As expected from results in Zhang et al. (2013) for urban and suburban Paris sites, the VBS-LA simulation with single-step oxidation scheme for ASOA and BSOA formation generally underestimates OA measurements, in particular for the background concentrations, by up to 80% (Fig. 5). A slight overestimation of 1 µg $m^{-3}$ is observed in the plume for the maximum concentration during the flight on the 16th. This is related to high POA and SI-SOA contributions to the total OA concentrations by up to 70% in the plume (Fig. S3 and S4). Thus apparently, the increased plume SI-SOA build-up due to increased POA emissions in the agglomeration is able to over compensate lack in background SOA at least for this day.

Simulations with the VBS-HNOX configuration show lower plume concentrations than those with the VBS-LNOX configuration, because of lower yields in SOA formation in the inner MEG3 domain. Background simulations are similar for both simulations corresponding to low $NO_x$ yields chosen for both simulation configurations in the larger domain. The maximum concentration of OA simulated with VBS-LNOX is overestimated with respect to the measurement by 1.7 (28%), 0.4 (3%) and 1.5 µg $m^{-3}$ (21%) on 16th, 21st and 29th, respectively, while it fits well with the observations in VBS-HNOX, being slightly underestimated by -0.5 (-8%), -1 (-8%) and -0.5 µg $m^{-3}$ (-7%) (Table 3 and S1, Fig. 5). The modeled OA background concentrations are underestimated both on 16th and on 29th by VBS-LNOX, by respectively -1.6 (-41%) and -1.0 µg $m^{-3}$ (-25%), and VBS-HNOX, by respectively -1.9 (-50%) and -1.4 µg $m^{-3}$ (-33%). They are overestimated with both configurations on the 21st, by 2.3 (36%) and 1.9 µg $m^{-3}$ (29%), respectively (Table 3 and S1). All in all, simulated and observed OA concentrations are rather similar, which is a satisfying result in light of often very large model to observation differences reported in literature (e.g. Sciare et al. 2010 for the Paris region). However, as the primary pollutants are generally underestimated by the model, this might be the result of compensating errors for different OA compounds. In a later section (4.3), we will thus rely on OA versus $O_x$ slopes in the Paris plume for further analysis.

### 4.2 OA plume build-up

First, the plume productions of OA (and of $O_x$) are derived here from the difference between maximum and background (30th percentile) concentrations over flight transects as

given in the last section. $O_x$ is preferred here with respect to $O_3$ since it is not affected by titration with NO. For the three flight days (16th, 21st and 29th), measured values of OA plume build-up are 2.1, 5.9 and 3.2 µg $m^{-3}$, respectively, while they are 5.4, 4.0 and 5.8 µg $m^{-3}$ in VBS-LNOX, 3.5, 3.0 and 4.1 µg $m^{-3}$ in VBS-HNOX and 5.9, 1.4 and 3.1 µg $m^{-3}$ in VBS-LA (Table 1 and 3). Thus, independent of the model configuration used, overestimations of plume OA occur on two days (16th and 29th), while an underestimation appears on the 21st. The plume $O_x$ production, calculated again from the difference between the maximum concentrations and the background concentrations are 12.9, 21.8 and 12.6 ppb from the measurements and 18.3, 14.4 and 18.8 ppb from VBS-LNOX, 22.5, 13.9 and 19.7 ppb from VBS-LA, again for the three flight days respectively (Table 1 and 3). As for OA, we encounter an overestimation of plume $O_x$ for the 16th and 29th, and an underestimation for the 21st. This suggests that the representation of photochemical conditions might be partially responsible for differences observed for OA, and thus that the given data set could not be used directly for evaluation of the OA scheme in the model.

To overcome these problems, we analyze here OA versus $O_x$ plots. As explained in the introduction, the slopes of these plots can represent in plume OA build-up, normalized with respect to the availability of VOC precursors and oxidant agents (OH, $O_3$ and $NO_3$). This holds under the ideal hypothesis of a constant mix of VOC, SVOC and IVOC precursors on one hand, and oxidant agents on the other hand, for the considered data points of a flight. As explained in section 2, we did not plot OOA or SOA vs. $O_x$ because of uncertainties related on PMF analysis and definition of HOA comparing to POA or/and SI-SOA and cooking related OA. In section 2, we also presented correlations of about 0.7 (R) between OA and $O_x$ measured on the flight legs for a given day. Modeled OA and $O_x$ on these flight legs show an even higher correlation of about 0.87 from VBS-LA except for 0.67 on 21st and more than 0.95 from VBS-HNOX and VBS-LNOX (Table 4). These good correlations suggest that we are close enough to the "constant mix" hypothesis to make the OA vs. $O_x$ slope a useful metrics. The simulated slopes of $OA/O_x$ are 0.23, 0.29 and 0.26 µg $m^{-3}$ $ppb^{-1}$ with the VBS-LNOX configuration for the three flights on 16th, 21st and 29th, respectively (Fig. 6, Table 5). They overestimate the measured slopes of 0.13, 0.14 and 0.15 µg $m^{-3}$ $ppb^{-1}$ by a factor between 1.7 and 2. It is noticed that the small variability in the relative differences between flights due to the normalizing method (i.e. plotting OA vs. $O_x$ to normalize with respect to photochemical conditions). This overestimation can be related to the SOA formation scheme: it is likely that the high SOA yields under low-$NO_x$ conditions are incorrect under plume conditions. The corresponding slopes in the VBS-HNOX simulation with lower yields under high $NO_x$ conditions are 0.15, 0.24 and 0.19 µg $m^{-3}$ $ppb^{-1}$, respectively. These slopes show a

much lower overestimation of a factor of 1.1, 1.7 and 1.3 for the three days. As for VBS-LA, the simulated $OA/O_x$ slope is overestimated by 46% on 16$^{th}$ with up to 70% of contribution of SI-SOA to the total OA, while it is underestimated by 50% and 27% on 21$^{st}$ and 29$^{th}$, respectively (Table 5). Thus, for all of the three flights, simulated $OA/O_x$ slopes with both VBS-HNOX and VBS-LA show a similar range of errors with respect to observed slopes (even if the sign of errors is different). However, as we will show in section 5, these two simulations show a very different distribution of ASOA, BSOA and SI-SOA build-up in the plume (Fig. S4, S5 and S6). Apparently, observed $OA/O_x$ slopes cannot constrain these distributions.

The measured slopes of OA vs. $O_x$ during the first two flight legs on these days are close to the ones during the last two flight legs (Fig. S7 and S8). In this analysis, VBS-HNOX is focused. The modeled slopes of OA vs. $O_x$, 0.12, 0.23 and 0.17 µg m$^{-3}$ ppb$^{-1}$ (for the 3 flights) are close to the measured ones (0.12, 0.18 and 0.16 µg m$^{-3}$ ppb$^{-1}$) during the first two flight legs. On the contrary, these slopes, 0.17, 0.25 and 0.21 µg m$^{-3}$ ppb$^{-1}$ are overestimated by a factor of 1.3, 1.9, and 1.3 with respect to the measured ones during the last two flight legs. Thus, the overestimation of slopes occurs especially during the last two flight legs. It is related to relatively higher anthropogenic SOA formation due to continuous chemical aging when the flights are farther away from Paris fresh emissions. Higher slopes during the last two flight legs than those during the first two flight legs are not seen for BSOA, probably because the biogenic VOC emissions are more diffuse (Fig. S7 and S8). Even if some differences are made evident, such a good agreement in OA vs. $O_x$ slopes between simulations and measurements represents a valuable validation of the VBS-HNOX scheme for the conditions of the Paris plume.

## 5. Impact of Paris plume on surrounding regions

In this section, we analyse the contribution of OA build-up from emissions in or near the Paris agglomeration to regional OA levels. This analysis is based on simulations with the VBS-HNOX configuration and the VBS-LA simulations which show similar errors with respect to observed $OA/O_x$ slopes indicative for plume OA build-up. The VBS-LNOX simulation clearly showed larger errors. We will first analyse the individual build-up of OA species for the three flight days (section 5.1), then we will study the time evolution of a pollution plume on the 16$^{th}$ of July (section 5.2), and finally, we present average results for July 2009.

## 5.1 Plume build-up of individual OA species

- *VBS-HNOX simulation*

The slopes of modeled SI-SOA, ASOA (anthropogenic SOA) and BSOA (biogenic SOA) versus $O_x$ are well correlated, generally with $R > 0.7$ (Table 4, Fig. 6). They are used here to analyze the plume production of individual OA species. SI-SOA is formed by functionalization and condensation of evaporated POA and IVOC species (Robinson et al., 2007) which are thought to be constituted by long alkane chains. SI-SOA vs. $O_x$ slopes are 0.04, 0.02, and 0.03 µg $m^{-3}$ $ppb^{-1}$ for the three flights, respectively (Table 5). They represent 27, 8, and 16% of the total OA vs. $O_x$ slopes. Thus SI-SOA has only a minor contribution to Paris plume OA formation in this simulation. The anthropogenic photochemical production of ASOA from aromatics dominates the OA production on 16$^{th}$ and 29$^{th}$, with slopes of 0.10 and 0.09, respectively, and of 0.08 µg $m^{-3}$ $ppb^{-1}$ on the 21$^{st}$ (Table 5). On the 29$^{th}$ and especially on 16$^{th}$, the SOA production is strongly influenced by anthropogenic emissions (by more than 90%). A major contribution of anthropogenic VOC emissions to OA build-up in the Paris plume during MEGAPOLI flights has also been found by Freney et al. (2014), from a conjoint analysis by AMS OA measurements, and PTR-MS VOC compounds. These results imply important SOA formation from the Paris agglomeration VOC and to a lesser extent POA/SI-VOC emissions. Borbon et al. (2013) found emission ratios for C7–C9 aromatics in Paris which were by a factor of 2–3 higher than in Los Angeles and other French and European Union urban areas. This clearly could favor large anthropogenic SOA formation to OA in the Paris plume. On the contrary, BSOA formation dominates the SOA production on 21$^{st}$, with a slope of BSOA vs. $O_x$ of 0.15 µg $m^{-3}$ $ppb^{-1}$ (Table 5), about 63% of the slope of OA vs. $O_x$. BSOA formation can both be due to fresh BVOC emissions from mainly isoprene emitting forests north of Paris or from condensation of biogenic SVOC when temperatures decrease in the later afternoon. Recently, the comparison of different VBS based SOA schemes to chamber measurements in Zhao et al. (2015) suggests lower SOA formation from traditional VOC precursors (ASOA), by explicitly simulating the first generation products, than when using the parametrization from Lane et al. (2008a) as in our study. In addition, Lane et al. (2008a) do not account for BSOA chemical aging, while we do based on the results of Zhang et al. (2013). Thus, the relative contributions of ASOA and BSOA to plume SOA build-up in the VBS-LNOX and VBS-HNOX configurations used in this paper are considered as an upper limit, while the primary SI-VOC emissions for SI-SOA formation are considered as a lower limit. Others studies taking into account fragmentation reactions (Jimenez et al. 2009; Shrivastava et al. 2011; Murphy et al. 2012) reduces OA formation.

- *VBS-LA simulation*

In the alternative VBS-LA simulation, the contribution of SI-SOA to the total slopes is dominating except for 21st (Table 5 and Fig. 6). SI-SOA vs. $O_x$ slopes are 0.15, 0.03, and 0.07 µg $m^{-3}$ $ppb^{-1}$ for the three flights, respectively and represent 79, 42, and 64% of the total OA vs. $O_x$ slopes. ASOA vs. $O_x$ slopes are negligible (0.00 or 0.01 µg $m^{-3}$ $ppb^{-1}$). BSOA vs. $O_x$ slopes are 0.02, 0.03, and 0.03 µg $m^{-3}$ $ppb^{-1}$ for the three flights, respectively and represent 10, 42, and 27% of the total OA vs. $O_x$ slopes. However it is noticed, for the VBS-LA simulation, the uncertainty in the determination of the slope is larger than for VBS-HNOX. For all three SI-SOA vs. $O_x$ plots, two regimes with two different slopes are observed. If the slope was only taken for points with larger SI-SOA and $O_x$ values, which are closer to the plume, a larger slope would have been determined. To a lesser extent, this feature also appears for VBS-LNOX simulations.

The larger SI-SOA vs. $O_x$ slopes in the VBS-LA simulation are easily explained by the larger POA emissions in this configuration. The range of SI-SOA vs. $O_x$ slopes between the VBS-HNOX and the VBS-LA configuration thus represents uncertainty due to POA emissions (Table 5). Even larger SI-SOA vs. $O_x$ slopes during these flights would be expected also if the more aggressive SI-SOA formation scheme by Grieshop et al. (2009) had been used. With the Grieshop et al. (2009) formulation, SVOC species have a reaction rate constant two times lower than in this study with Robinson et al. (2007), but are shifted to two orders of magnitude lower volatility (instead of one), with a mass increase by 40% for each oxidation step (instead of 7.5%). Box simulations by Dzepina et al. (2011) for Mexico City and by Hayes et al. (2015) for Los Angeles yield about two times larger SI-SOA yields with the Grishop et al. (2009) than with the Robinson et al. (2007) scheme. These results suggest an additional possibility to increase SI-SOA contributions to plume SOA.

As a result of these comparisons, we come to the conclusion that due to uncertainty both in POA emissions, and in the SOA formation formulations, the constraint of observed OA vs. $O_x$ slopes is on the SOA product distribution in the Paris plume is unfortunately weak. Both ASOA and SI-SOA could be the major anthropogenic SOA products for two flights, with varying contributions of BSOA.

## 5.2 Time evolution of the plume on July 16th

Fig. 7 gives a typical picture of the OA species evolution in the Paris plume (at surface), simulated with both the VBS-HNOX scheme and the VBS-LA scheme.

With the VBS-HNOX scheme, on July 16$^{th}$ at 7 UTC, a morning peak of OA is formed inside the Paris agglomeration as a result of POA emissions, low wind speeds, and a low boundary layer height. This peak of OA is then transported northeast. It disappears in the later morning (10 UTC) due to an increase of the PBL height and stronger winds. In the early afternoon (13 UTC), an OA plume is formed at about 50 km from the agglomeration center due to photochemical SOA production. At 16 UTC, the plume travels further north-east. Largest OA values occur between 49.5°N and 50°N, about 100 km north of Paris, in agreement with measurements. Major contributors ASOA and SI-SOA add more than 5 and 2 µg m$^{-3}$ of OA to the plume maximum (Fig. 8). The ASOA and SI-SOA plumes are clearly separated from the Paris agglomeration, because of (i) the time needed for processing of precursor emissions, and (ii) the largest accumulation of precursor emissions in the early morning hours when wind speeds over the agglomeration were very low (also seen in the POA peak at the same location). BSOA contributes to the regional background and is little affected by anthropogenic Paris agglomeration emissions (Fig. 8). The highest OA concentrations of about 10 µg m$^{-3}$ occurs in the evening at 19 UTC in northern France (at ~150 km distance from the agglomeration center) due to continuous photochemical SVOC production and aging, and due to lower temperatures. At 22 UTC, the plume is leaving the MEG3 model domain.

This phenomenon of continuing SOA formation which is detached from the original rush hour emission area due to transport is very similar to that observed for Los Angeles in the CalNex study (Hayes et al., 2013).

The corresponding results obtained with the VBS-LA scheme are shown in the Supplementary Material (Fig. S9). Morning OA concentrations are about three times larger than in VBS-HNOX due to larger emissions, while the background concentrations are all lower than 1 µg m$^{-3}$. At 13 UTC, an OA plume with concentrations of about 6 µg m$^{-3}$ slightly higher than in VBS-HNOX is formed at about 50 km from the agglomeration center. While ASOA is the major contributor to OA plume formation in VBS-HNOX, SI-SOA formation contributes the most to the plume in VBS-LA and produces the maximum concentration of about 6 µg m$^{-3}$ in the later afternoon at 16 UTC towards the northern France. POA, ASOA or BSOA contribute less than 1 µg m$^{-3}$ to the OA plume maximum (Fig. S10).

### 5.3 Average July 2009 urban OA contribution to the surroundings of Paris

Here, we analyze the regional scale OA build-up from the Paris emissions for the average of July 2009 from the VBS-HNOX (Fig. 9, 10)and VBS-LA simulation (Fig. S11 and S12). For VBS-HNOX, average OA concentrations around the Paris agglomeration do not show distinctive pollution plumes, but instead a strong W-E gradient near the agglomeration, presumably due to averaging different plume directions, and due to differences in background conditions. OA values also show strong decreasing gradients at about 100 to 150 km in the N-NE of Paris. Contrary to VBS-HNOX, OA values from VBS-LA show a distinct OA plume from the Paris agglomeration, absolute plume concentrations are lower. This behavior can be analyzed by considering specifically the contributions to OA.

For the VBS-HNOX simulation, average POA from Paris emissions is only about 0.15 µg $m^{-3}$ over Paris and the area of enhanced values is extending to E / NE because of the largest climatological frequency of south-westerly to westerly winds in July (Fig. 10). The areas of enhancements of POA occur on a length scale of some tens of kilometers around the agglomeration. ASOA is enhanced within the agglomeration and within the SW and NNE plume, up to 100 to 150 km downwind the agglomeration respectively. The maximum concentrations in these plumes are 0.4 and 0.35 µg $m^{-3}$, respectively (always for the July 2009 average). In the NNE direction, enhanced values originate from pollution events under SW flow such as those studied in this work (see section 5.2). The enhanced values in the SW originate from a pronounced pollution plume occurring in the beginning of July, for which no measurements were available. SI-SOA is most enhanced in the NNE direction where its maximum concentration is about 0.35 µg $m^{-3}$, thus somewhat smaller than the ASOA concentration. It is worth noting that these increases in ASOA and SI-SOA concentrations are much larger when analyzing individual events than when looking at averages, due to different plume angles on different days, thus diluting the average fields. The BSOA component does not show distinct plumes, but a continuous NW/W – SE/E gradient, that is the continental character of air masses implies large average BSOA concentrations. BSOA is the strongest contributor to OA over the domain. Its gradient is responsible for the W-E OA gradient noticed earlier, with smaller contributions from the other components.

For the VBS-LA simulation, the larger primary S/IVOC emissions within the LA inventory lead to larger average POA concentration, up to 0.7 µg $m^{-3}$ within the Paris agglomeration. Monthly maximum plume SI-SOA concentration is about 0.3 µg $m^{-3}$ in VBS-LA (Fig. S12). The lower SI-SOA concentration albeit higher POA concentrations is due to lower OA load in the plume. Indeed, monthly average plume ASOA concentration is small,

638 below 0.05 µg $m^{-3}$, plume BSOA concentration is below 0.3 µg $m^{-3}$. BSOA shows a similar
639 spatial pattern in VBS-LA, but with lower absolute values than in VBS-HNOX.

640 In conclusion, both the VBS-HNOX and VBS-LA simulations show different monthly
641 average OA product distributions. As discussed above, the ASOA and BSOA contributions in
642 VBS-HNOX represent an upper limit for ASOA and BSOA produced in the plume (and in
643 background airmasses). On the contrary the small plume and background values in VBS-LA
644 simulated without any chemical aging are probably underestimated, in particular because they
645 underestimate the SOA observations within the Paris agglomeration (Zhang et al., 2013). On
646 the contrary, for SI-SOA, differences between both simulations are weak. However,
647 alternative VBS schemes (Grishop et al., 2009) would simulate higher SI-SOA formation, as
648 noted above (about a factor two from box model studies in other urban plumes).

649

650 **6. Conclusion**

651 CHIMERE simulations are used to study the secondary pollutant formation in the
652 Paris plume and its impact on the surrounding regions. This study focusses on three photo-
653 chemically active days for which airborne observations are available. Three simulation
654 configurations are set-up in order to cover the range of uncertainty in emissions and in
655 different formulations of the SOA build-up in the frame of the VBS scheme. Primary
656 pollutants within the plume, such as $NO_x$ and BC, and probably also POA, are clearly
657 underestimated in the model when using the MEGAPOLI inventory, and to a lesser extent
658 with the EMEP-LA inventory. For two of the three flights, this underestimation is probably
659 due to too high wind speeds in the morning over the Paris agglomeration not allowing for
660 strong enough pollution accumulation. On the contrary, ozone is slightly overestimated in the
661 plume and in background airmasses, as is $O_x$. This is not contradictory since the chemical
662 regime in Paris and its surrounding is generally $NO_x$ saturated (Deguillaume et al., 2008).
663 Both in observations and simulations, predicted (and measured) OA is very well correlated
664 with predicted (and measured) $O_x$. The ratio of the photochemical productivities of SOA and
665 $O_x$ (represented by the slope of OA vs. $O_x$) is well simulated (overestimation of less than 30%
666 on the average of three days) for the Paris plume from VBS-HNOX when low SOA yields are
667 applied on the SOA formation scheme. The overestimation might be related to too large
668 yields of ASOA in the VBS scheme set-up in this work which was based on the parameters
669 given in Lane et al. (2008a) and Murphy et al., (2009). Nevertheless, this good agreement is
670 an important result in evaluating the VBS scheme with field data. Combined with similar

recent results for the Tokyo megacity (Morino et al., 2014), it shows good performance of the VBS schemes in large urban areas or their plumes. When considering the OA to $O_x$ slopes, the day to day variability in model to observation results is much lower than for OA alone. Observed OA vs $O_x$ slopes of about 0.14 to 0.15 µg $m^{-3}$ $ppb^{-1}$ compare well to those observed in the Mexico City, the Los Angeles and the Tokyo plumes with different emissions and photochemical conditions during different season (Fig. 1).

However, an alternative scheme with three times larger POA emissions, and without ASOA and BSOA aging, also shows good agreement with observed OA vs $O_x$ slopes, though it strongly underestimates background and urban Paris OA. This leads us to the conclusion that due to uncertainties both in POA emissions and in the SOA formation formulations, uncertainly in the SOA product distribution remains large. The constraint of observed OA vs. $O_x$ slopes on the SOA product distribution in the Paris plume is unfortunately weak, and does not reduce this uncertainty (while it does for anthropogenic OA yields). Both ASOA and SI-SOA could be the major anthropogenic SOA products for two flights. In the simulations anthropogenic SOA is the major contributor to plume SOA on two flight days, while BSOA is major or equivalent on the third day.

Predicted maximum OA is found on the flight leg most distant from the agglomeration (at about 150 km), as for observations, indicating secondary anthropogenic SOA formation from Paris emissions over all the distances and during several hours. On a monthly average, OA from Paris emissions contributes to the OA regional build-up at different length scales, from several tens for POA to several hundreds of kilometers for ASOA and SI-SOA. Clearly, a combination of ASOA and SI-SOA build-up from precursor emissions in the Paris agglomeration affects atmospheric composition at regional scale. Simulating this build-up has been possible only after an original model evaluation showing good agreement between simulated and observed OA to $O_x$ slopes. This slope is an interesting parameter to measure the SOA build-up efficiency of a given environment.

**Acknowledgements**

The research leading to these results has received funding from the European Community's Seventh Framework Programme FP/2007-2011 under grant agreement n°212520. Support from the French ANR project MEGAPOLI – PARIS (ANR-09-BLAN-0356), from the CNRS-INSU/FEFE via l'ADEME (n° 0962c0018) and the Ile de France/SEPPE are acknowledged. We would like to thank the pilots, the flight crew, and the whole SAFIRE

team for operating the ATR-42 aircraft. A part of the work was supported by a PhD grant from French CIFRE (ANRT) to Q.J. ZHANG (at LISA/CNRS and ARIA Technologies).

**References**

Aumont, B., Valorso, R., Mouchel-Vallon, C., Camredon, M., Lee-Taylor, J., and Madronich, S. (2012): Modeling SOA formation from the oxidation of intermediate volatility *n*-alkanes, Atmos. Chem. Phys., 12, 7577-7589.

Beekmann, M., and Vautard, R. (2010): A modelling study of photochemical regimes over Europe: robustness and variability, Atmos. Chem. Phys., 10, 10067-10084.

Beekmann, M., Prévôt, A. S. H., Drewnick, F., Sciare, J., Pandis, S. N., Denier van der Gon, H. A. C., Crippa, M., Freutel, F., Poulain, L., Ghersi, V., Rodriguez, E., Beirle, S., Zotter, P., von der Weiden-Reinmüller, S.-L., Bressi, M., Fountoukis, C., Petetin, H., Szidat, S., Schneider, J., Rosso, A., El Haddad, I., Megaritis, A., Zhang, Q. J., Michoud, V., Slowik, J. G., Moukhtar, S., Kolmonen, P., Stohl, A., Eckhardt, S., Borbon, A., Gros, V., Marchand, N., Jaffrezo, J. L., Schwarzenboeck, A., Colomb, A., Wiedensohler, A., Borrmann, S., Lawrence, M., Baklanov, A., and Baltensperger, U. (2015): In situ, satellite measurement and model evidence on the dominant regional contribution to fine particulate matter levels in the Paris megacity, Atmos. Chem. Phys., 15, 9577-9591

Bessagnet, B., Menut, L., Curci, G., Hodzic, A., Guillaume, B., Liousse, C., Moukhtar, S., Pun, B., Seigneur, C., and Schulz, M. (2009): Regional modeling of carbonaceous aerosols over Europe – focus on secondary organic aerosols, J. Atmos. Chem., 61, 175– 202.

Borbon, A., Gilman, J.B., Kuster, W. C., Grand, N., Chevaillier, S., Colomb, A., Dolgorouky, C., Gros, V., Lopez, M., Sarda-Esteve, R., Holloway, J., Stutz, J., Perrussel, O., Petetin, H., McKeen, S., Beekmann, M., Warneke, C., Parrish D.D., and de Gouw, J.A., (2013): Emission ratios of anthropogenic VOC in northern mid-latitude megacities: observations vs. emission inventories in Los Angeles and Paris, J. Geophys. Res., 118, 2041-2057.

Derognat, C., Beekmann, M., Baeumle, M., Martin, D., and Schmidt, H. (2003): Effect of biogenic volatile organic compound emissions on tropospheric chemistry during the atmospheric Pollution Over the Paris Area(ESQUIF) campaign in the Ile-de-France region. J. Geophys. Res., 108(D17):8560.

Cappa, C. D. and Wilson, K. R.: Multi-generation gas-phase oxidation, equilibrium partitioning, and the formation and evolution of secondary organic aerosol, Atmos. Chem. Phys., 12, 9505-9528, 2012.

Crippa, M., DeCarlo, P. F., Slowik, J. G., Mohr, C., Heringa, M. F., Chirico, R., Poulain, L., Freutel, F., Sciare, J., Cozic, J., Di Marco, C. F., Elsasser, M., Nicolas, J. B., Marchand, N., Abidi, E., Wiedensohler, A., Drewnick, F., Schneider, J., Borrmann, S., Nemitz, E., Zimmermann, R., Jaffrezo, J.-L., Prévôt, A. S. H., and Baltensperger, U.: Wintertime aerosol chemical composition and source apportionment of the organic fraction in the metropolitan area of Paris, Atmos. Chem. Phys., 13, 961-981, 2013

Donahue, N. M., Robinson, A. L., Stanier, C. O., and Pandis, S. N., (2006): Coupled partitioning, dilution, and chemical aging of semivolatile organics, Environ. Sci. Technol., 40, 2635–2643.

745 Dudhia, J. (1993): A nonhydrostatic version of the Penn State/NCAR mesoscale model: validation
746 tests and simulation of an Atlantic cyclone and cold front, Mon. Weather Rev., 121, 1493–
747 1513.
748 Dzepina, K., Cappa, C.D., Volkamer, R.M., Madronich, S., DeCarlo, P.F., Zaveri, R.A., and Jimenez,
749 J.L. (2011): Modeling the Multiday Evolution and Aging of Secondary Organic Aerosol
750 During MILAGRO 2006. Environmental Science and Technology, 45, 3496-3503,
751 doi:10.1021/es103186
752 Freney, E. J., Sellegri, K., Canonaco, F., Colomb, A., Borbon, A., Michoud, V., Doussin, J.-F.,
753 Crumeyrolle, S., Amarouche, N., Pichon, J.-M., Bourianne, T., Gomes, L., Prevot, A. S. H.,
754 Beekmann, M., and Schwarzenböeck, A., (2014): Characterizing the impact of urban
755 emissions on regional aerosol particles: airborne measurements during the MEGAPOLI
756 experiment, Atmos. Chem. Phys., 14, 1397-1412.
757 Guenther, A., Karl, T., Harley, P., Wiedinmyer, C., Palmer, P. I., and Geron, C., (2006): Estimates of
758 global terrestrial isoprene emissions using MEGAN (Model of Emissions of Gases and
759 Aerosols from Nature), Atmos. Chem. Phys., 6, 3181–3210.
760 Gurjar, B.R., Jain, A., Sharma, A., Agarwal, A., Gupta, P.,Nagpure, A.S. and Lelieveld, J., (2010):
761 Human health risksin megacities due to air pollution, Atmos. Env. 44, 4606-4613.
762 Hallquist, M., Wenger, J. C., Baltensperger, U., Rudich, Y., Simpson, D., Claeys, M., Dommen, J.,
763 Donahue, N. M., George,C., Goldstein, A. H., Hamilton, J. F., Herrmann, H., Hoffmann, T.,
764 Iinuma, Y., Jang, M., Jenkin, M. E., Jimenez, J. L.,Kiendler-Scharr, A., Maenhaut, W.,
765 McFiggans, G., Mentel, Th. F., Monod, A., Prévot, A. S. H., Seinfeld, J. H., Surratt, J. D.,
766 Szmigielski, R., and Wildt, J., (2009): The formation, properties and impact of secondary
767 organic aerosol: current and emerging issues, Atmos. Chem. Phys., 9, 5155–5236.
768 Hauglustaine, D. A., Hourdin, F., Jourdain, L., Filiberti, M. A., Walters, S., Lamarque, J.-F., and
769 Holland, E. A.: Interactive chemistry in the Laboratoire de Meteorologie. Dynamique general
770 circulation model, (2004): Description and background tropospheric chemistry evaluation, J.
771 Geophys. Res., 109, D04314, doi:10.1029/2003JD003957.
772 Hayes, P. L., Ortega, A. M., Cubison, M. J., Froyd, K. D., Zhao, Y., Cliff, S. S., Hu, W. W., Toohey,
773 D. W., Flynn, J. H., Lefer, B. L., Grossberg, N., Alvarez, S., Rappenglück, B., Taylor, J. W.,
774 Allan, J. D., Holloway, J. S., Gilman, J. B., Kuster, W. C., Gouw, J. A., Massoli, P., Zhang,
775 X., Liu, J., Weber, R. J., Corrigan, A. L., Russell, L. M., Isaacman, G., Worton, D. R.,
776 Kreisberg, N. M., Goldstein, A. H., Thalman, R., Waxman, E. M., Volkamer, R., Lin, Y. H.,
777 Surratt, J. D., Kleindienst, T. E., Offenberg, J. H., Dusanter, S., Griffith, S., Stevens, P. S.,
778 Brioude, J., Angevine, W. M., Jimenez, J. L. (2013): Organic aerosol composition and sources
779 in Pasadena, California during the 2010 CalNex campaign, J. Geophys. Res. Atmos., 118,
780 9233–9257, doi:10.1002/jgrd.50530
781 Hayes, P. L., Carlton, A. G., Baker, K. R., Ahmadov, R., Washenfelder, R. Alvarez, A., S.,
782 Rappenglück, B., Gilman, J. B., Kuster, W. C., de Gouw, J. A., Zotter, P., Prévôt, A. S. H.,
783 Szidat, S., Kleindienst, T. E., Offenberg, J. H., and Jimenez, J. L. (2015): Modeling the
784 formation and aging of secondary organic aerosols in Los Angeles during CalNex 2010,
785 Atmos. Chem. Phys., 15, 5773-5801
786 Herndon, S., Onasch, T., Wood, E. C., Kroll, J. H., Canagaratna,M., Jayne, J., Zavala, M., Knighton,
787 W. B., Mazzoleni, C.,Dubey, M. K., Ulbrich, I., Jimenez, J. L., Seila, R., de Gouw,J. A., De
788 Foy, B., Fast, J., Molina, L., Kolb, C. E., and Worsnop, D. R. (2008): The correlation of

secondary organic aerosol with odd oxygen in Mexico City, Geophys. Res. Lett, 35, L15804, oi:10.1029/2008GL034058.

Hodzic, A., Jimenez, J. L., Madronich, S., Canagaratna, M. R., DeCarlo, P. F., Kleinman, L., and Fast, J., (2010): Modeling organic aerosols in a megacity: potential contribution of semi-volatile and intermediate volatility primary organic compounds to secondary organic aerosol formation, Atmos. Chem. Phys., 10, 5491–5514.

Honoré, C. , Rouil, L., Vautard, R., Beekmann, M., Bessagnet, B., Dufour, A., Elichegaray, C., Flaud, J.-M., Malherbe, L., Meleux, F., Menut, L., Martin, D., Peuch, A., Peuch, V. H., and Poisson, N. (2008): Predictability of European air quality: The assessment of three years of operational forecasts and analyses by the PREV'AIR system, J. Geophys. Res., 113, D04301, doi:10.1029/2007JD008761.

IPCC: Climate Change 2013: The Physical Science Basis: Summary for Policymakers, Cambridge, UK, 2013

Jimenez, J. L., Canagaratna, M. R., Donahue, N. M., Prevot, A. S. H., Zhang, Q., Kroll, J. H., DeCarlo, P. F., Allan, J. D., Coe, H., Ng, N. L., Aiken, A. C., Docherty, K. S., Ulbrich, I. M., Grieshop, A. P., Robinson, A. L., Duplissy, J., Smith, J. D., Wilson, K. R., Lanz, V. A., Hueglin, C., Sun, Y. L., Tian, J., Laaksonen, A., Raatikainen, T., Rautiainen, J., Vaattovaara, P., Ehn, M., Kulmala, M., Tomlinson, J. M., Collins, D. R., Cubison, M. J., Dunlea, E. J., Huffman, J. A., Onasch, T. B., Alfarra, M. R., Williams, P. I., Bower, K., Kondo, Y., Schneider, J., Drewnick, F., Borrmann, S., Weimer, S., Demerjian, K., Salcedo, D., Cottrell, L., Griffin, R., Takami, A., Miyoshi, T., Hatakeyama, S., Shimono, A., Sun, J. Y., Zhang, Y. M., Dzepina, K., Kimmel, J. R., Sueper, D., Jayne, J. T., Herndon, S. C., Trimborn, A. M., Williams, L. R., Wood, E. C., Middlebrook, A. M., Kolb, C. E., Baltensperger, U., and Worsnop, D. R. , (2009): Evolution of Organic Aerosols in the Atmosphere, Science, 326, 1525–1529, doi:10.1126/science.1180353.

Junker, C. and Liousse, C., (2008): A global emission inventory of carbonaceous aerosol from historic records of fossil fuel and biofuel consumption for the period 1860-1997, Atmos. Chem. Phys., 8, 1195–1207.

Kleinman, L. I., P. H. Daum, J. H. Lee, Y.-N. Lee, L. J. Nunnermacker, S. R. Springston, L. Newman, J. Weinstein-Lloyd, S. Sillman, (1997), Dependence of ozone production on NO and hydrocarbons in the troposphere, Geophys. Res. Lett., 24, 2299-2302.

Lane, T. E.; Donahue, N. M.; Pandis, S. N., (2008a): Simulating secondary organic aerosol formation using the volatility basis-set approach in a chemical transport model. Atmos. Environ., 42, 7439– 7451.

Lane, T. E., Donahue, N. M., and Pandis, S. N., (2008b): Effect of NOx on secondary organic aerosol concentrations, Environ. Sci. Technol., 42, 6022–6027.

Lattuati, M. (1997): Contribution à l'étude du bilan de l'ozone troposphérique à l'interface de l'Europe et de l'Atlantique Nord: modélisation lagrangienne et mesures en altitude. Thèse de sciences, Université Paris 6, France

Menut L, Bessagnet, B., Khvorostyanov, D., Beekmann, M., Blond, N., Colette, A., Coll, I., Curci, G., Foret, G., Hodzic, A., Mailler, S., Meleux, F., Monge, J.L., Pison, I., Siour, G., Turquety, S., Valari, M., Vautard, R.and Vivanco, M.G., (2013): CHIMERE 2013: a model for regional atmospheric composition modelling, Geoscientific Model Development, 6, 981-1028, doi:10.5194/gmd-6-981-2013

Molina, L. T., Madronich, S., Gaffney, J. S., Apel, E., de Foy, B.,Fast, J., Ferrare, R., Herndon, S., Jimenez, J. L., Lamb, B., Osornio-Vargas, A. R., Russell, P., Schauer, J. J., Stevens, P. S., Volkamer, R., and Zavala, M.:An overview of the MILAGRO 2006 Campaign: Mexico City emissions and their transport and transformation, Atmos. Chem. Phys., 10, 8697-8760, 2010.

Morino, Y., K. Tanabe, K. Sato, and T. Ohara (2014), Secondary organic aerosol model intercomparison based on secondary organic aerosol to odd oxygen ratio in Tokyo, J. Geophys. Res. Atmos., 119, 13,489–13,505, doi:10.1002/2014JD021937

Murphy, B. N., Pandis, S. N., (2009): Simulating the formation of semivolatile primary and secondary organic aerosol in a regional chemical transport model. Environ. Sci. Technol. 43 (13), 4722–4728.

Nenes, A., Pilinis, C., and Pandis, S. (1998): ISORROPIA: A new thermodynamic model for inorganic multicomponent atmospheric aerosols. Aquatic Geochem., 4:123–152.

Petetin, H., Beekmann, M., Sciare, J., Bressi, M., Rosso, A., Sanchez, O., and Ghersi, V., (2014): A novel model evaluation approach focussing on local and advected contributions to urban PM2.5 levels – application to Paris, Geosci. Model Dev., 7, 1483-1505.

Petetin, H., Beekmann, M., Colomb, A., Denier van der Gon, H. A. C., Dupont, J.-C., Honoré, C., Michoud, V., Morille, Y., Perrussel, O., Schwarzenboeck, A., Sciare, J., Wiedensohler, A., and Zhang, Q. J. (2015): Evaluating BC and NOx emission inventories for the Paris region from MEGAPOLI aircraft measurements, Atmos. Chem. Phys., 15, 9799-9818

Pun, B. K., Seigneur, C., and Lohman, K., (2006): Modeling secondary organic aerosol formation via multiphase partitioning with molecular data, Environ. Sci. Technol., 40, 4722–4731, doi:10.1021/es0522736.

Robinson, A. L., Donahue, N. M., Shrivastava, M. K., Weitkamp, E. A., Sage, A. M., Grieshop, A. P., Lane, T. E., Pierce, J. R., and Pandis, S. N., (2007): Rethinking organic aerosols: Semivolatile emissions and photochemical aging, Science, 315(5816), 1259–1262.

Sciare J., d'Argouges O., Zhang Q. J., Sarda-Estève R., Gaimoz C., Gros V., Beekmann M., and Sanchez O., (2010) : Comparison between simulated and observed chemical composition of fine aerosols in Paris (France) during springtime: contribution of regional versus continental emissions, Atmos. Chem. Phys., 10, 11987–12004

Seinfeld, J. H. and Pandis, S. N. (2006): Atmospheric Chemistry and Physics: From Air Pollution to Climate Changes, John Wiley, Hoboken, N. J.

Shrivastava, M., Zelenyuk, A., Imre, D., Easter, R.C., Beranek,, J., Zaveri, R.A, and Fast, J.D. (2013): Implications of Low Volatility and Gas-phase Fragmentation Reactions on SOA Loadings and their Spatial and Temporal Evolution in the Atmosphere. J. Geophys. Res. Atmos., 118(8), 3328-3342, doi: 10.1002/jgrd.50160, 2013.

Shaiganfar, R., Beirle, S., Petetin, H., Zhang, Q.J., Beekmann, M., and Wagner T., (2015): New concepts for the comparison of tropospheric NO2 column densities derived from car-MAX-DOAS observations, OMI satellite observations and the regional model CHIMERE during two MEGAPOLI campaigns in Paris 2009/10, Atmos. Meas. Tech., 8, 2827-2852

Timmermans, R.M.A., Denier van der Gon, H.A.C., Kuenen, J.J.P., Segers, A.J., Honoré, C., Perrussel, O., Builtjes, P.J.H., and Schaap, M., (2013): Quantification of the urban air pollution increment and its dependency on the use of down-scaled and bottom-up city emission inventories, Urban Climate 6, 46-62.

United Nations: World Urbanization Prospects, the 2011 Revision, esa.un.org/unpd/wup/index.htm.

Vautard, R., Beekmann, M., Roux, J., and Gombert, D. (2001): Validation of a hybrid forecasting system for the ozone concentrations over the Paris region, Atmos. Environ., 35, 2449–2461.

Volkamer, R., Jimenez, J. L., Martini, F. S., Dzepina, K., Zhang, Q., Salcedo, D., Molina, L. T., Worsnop, D. R., and Molina, M. J., (2006): Secondary organic aerosol formation from anthropogenic air pollution: Rapid and higher than expected, Geophys. Res. Lett., 33, L17811, doi:10.1029/2006GL026899.

Wood, E.C., E. C., Canagaratna, M. R., Herndon, S. C., Onasch, T. B., Kolb, C. E., Worsnop, D. R., Kroll, J. H., Knighton, W. B., Seila, R., Zavala, M., Molina, L. T., DeCarlo, P. F., Jimenez, J. L., Weinheimer, A. J., Knapp, D. J., Jobson, B. T., Stutz, J., Kuster, W. C., and Williams, E. J. (2010): Investigation of the correlation between odd oxygen and secondary organic aerosol in Mexico City and Houston. Atmos. Chem. Phys. 10, 8947-8968.

Zhang, Q. J., Laurent, B., Velay-Lasry, F., Ngo, R., Derognat, C., Marticorena, B., Albergel, A., (2012) : An Air Quality Forecasting System in Beijing – Application to the Study of Dust Storm Events in China in May 2008, J. Environ. Sci., 10.1016/S1001-0742(11)60733-X .

Zhang, Q. J., Beekmann, M., Drewnick, F., Freutel, F., Schneider, J., Crippa, M., Prevot, A. S. H., Baltensperger, U., Poulain, L., Wiedensohler, A., Sciare, J., Gros, V., Borbon, A., Colomb, A., Michoud, V., Doussin, J.-F., Denier van der Gon, H. A. C., Haeffelin, M., Dupont, J.-C., Siour, G., Petetin, H., Bessagnet, B., Pandis, S. N., Hodzic, A., Sanchez, O., Honoré, C., and Perrussel, O. , (2013): Formation of organic aerosol in the Paris region during the MEGAPOLI summer campaign: evaluation of the volatility-basis-set approach within the CHIMERE model, Atmos. Chem. Phys., 13, 5767-5790.

Zhao, B., Wang, S., Donahue, N. M., Chuang, W., Hildebrandt Ruiz, L., Ng, N. L., Wang, Y., and Hao, J. (2015): Evaluation of One-Dimensional and Two-Dimensional Volatility Basis Sets in Simulating the Aging of Secondary Organic Aerosol with Smog-Chamber Experiments, Environ. Sci. Technol., 49, 2245-2254

907 **Table 1 Airborne chemical instruments deployed, the measurements including the maximum and**
908 **30$^{th}$ percentile (P30) of pollutant concentrations by these instruments are used to discuss general**
909 **findings during the campaign (Freney et al., 2014) and evaluate the model simulations.**

| Pollutant | Instrument | Time resolution | Unit | Statistics | Concentration | | |
|---|---|---|---|---|---|---|---|
| | | | | | 16$^{th}$ | 21$^{st}$ | 29$^{th}$ |
| $NO_x$ | MONA[1] | 30 s | ppb | Max. | 13.5 | 7.98 | 12.2 |
| | | | | P30 | 1.11 | 1.03 | 1.14 |
| $O_3$ | UV analyser[2] | 30 s | ppb | Max. | 62.0 | 79.0 | 62.4 |
| | | | | P30 | 49.0 | 58.0 | 50.0 |
| BC | PSAP[3] | 1 s | μg m$^{-3}$ | Max. | 2.00 | 2.01 | 2.30 |
| | | | | P30 | 0.33 | 0.49 | 0.38 |
| OA | C-ToF-AMS[4] | 30 s | μg m$^{-3}$ | Max. | 5.97 | 12.3 | 7.36 |
| | | | | P30 | 3.87 | 6.47 | 4.13 |

910 [1] Measurement of Nitrogen on Aircraft developed by the Laboratoire Interuniversitaire des Systems
911 Atmosphériques (LISA). NO, $NO_2$ and $NO_y$ are measured (Freney et al. 2014, Supplementary
912 Material).
913 [2] Thermal-environmental instruments $O_3$ UV analyzer
914 [3] Radiance research ® Particulate Soot Absorption Photometer
915 [4] Aerodyne Compact Time-of-flight Aerosol Mass Spectrometer
916

917 **Table 2 Secondary organic aerosol (SOA) mass yields used in this work. These yields are for**
918 **surrogate VOC species with saturation concentrations of 1, 10, 100 and 1000 μg m$^{-3}$ at 298 K**
919 **(Murphy and Pandis, 2009).**

| VOCs | VBS-LNOX with low-$NO_x$ condition | | | | VBS-HNOX with high-$NO_x$ condition | | | |
|---|---|---|---|---|---|---|---|---|
| | 1 | 10 | 100 | 1000 | 1 | 10 | 100 | 1000 |
| ALK4[1] | 0 | 0.075 | 0 | 0 | 0 | 0.0375 | 0 | 0 |
| ALK5[2] | 0 | 0.3 | 0 | 0 | 0 | 0.15 | 0 | 0 |
| OLE1[3] | 0.0045 | 0.009 | 0.06 | 0.225 | 0.0008 | 0.0045 | 0.0375 | 0.15 |
| OLE2[4] | 0.0225 | 0.0435 | 0.129 | 0.375 | 0.003 | 0.0255 | 0.0825 | 0.27 |
| ARO1[5] | 0.075 | 0.225 | 0.375 | 0.525 | 0.003 | 0.165 | 0.3 | 0.435 |
| ARO2[6] | 0.075 | 0.3 | 0.375 | 0.525 | 0.0015 | 0.195 | 0.3 | 0.435 |
| TERP[7] | 0.1073 | 0.0918 | 0.3587 | 0.6075 | 0.012 | 0.1215 | 0.201 | 0.507 |
| ISOP[8] | 0.009 | 0.03 | 0.015 | 0 | 0.0003 | 0.0225 | 0.015 | 0 |

920 [1] n-pentane, n-hexane, Branched C5-C6 Alkanes, Cyclopetane, Trimethyl Butane, Trimethyl Pentane,
921 Isopropyl alcool, n-Propyl Alcool
922 [2] C7-C22 n-Alkanes, C6-C16 Cycloalkanes, branched/Unspeciated C8-C18 Alkanes
923 [3] Propene, C4-C15 terminal Alkanes
924 [4] Isobutene, C4-C15 Internal Alkenes, C6-C15 Cyclic or di-olefins, Styrenes
925 [5] Toluene, benzene, Ethyl benzene, C9-C13 Monosubstituted Benzenes
926 [6] Xylenes, Ethyl Toluenes, Dimethyl and Trimethyl Benzenes, Ethylbezenes, naphthalene, C8-C13 Di-
927 , Tri-, Tetra-, Penta-, Hexa-substituted Benzenes, Unspeciated C10-C12 Aromatics
928 [7] α-pinene and sabinene, β-pinene and δ3-carene, limonene, ocimene and myrcene
929 [8] Isoprene

**Table 3 Model statistics for maximum and 30$^{th}$ percentile (P30) of pollutant concentrations from VBS-LNOX (and VBS-HNOX for OA as well) and VBS-LA**

| Pollutant | Unit | Statistics | VBS-LNOX | | | VBS-LA | | |
|---|---|---|---|---|---|---|---|---|
| | | | 16$^{th}$ | 21$^{st}$ | 29$^{th}$ | 16$^{th}$ | 21$^{st}$ | 29$^{th}$ |
| $NO_x$ | ppb | Max. | 9.18 | 2.82 | 4.92 | 6.16 | 2.25 | 3.54 |
| | | P30 | 0.47 | 0.61 | 0.55 | 0.62 | 0.67 | 0.63 |
| BC | μg m$^{-3}$ | Max. | 1.3 | 0.52 | 0.69 | 2.41 | 0.77 | 1.08 |
| | | P30 | 0.16 | 0.18 | 0.16 | 0.11 | 0.15 | 0.11 |
| $O_3$ | ppb | Max. | 69.5 | 83.3 | 70.7 | 74.9 | 83.3 | 72.2 |
| | | P30 | 53.3 | 69.3 | 53.0 | 53.6 | 69.7 | 53.3 |
| $O_x$ | ppb | Max. | 72.1 | 84.2 | 72.2 | 76.7 | 84.2 | 73.4 |
| | | P30 | 53.7 | 69.8 | 53.4 | 54.1 | 70.3 | 53.8 |
| OA | μg m$^{-3}$ | Max. | 7.66 | 12.74 | 8.87 | 6.97 | 3.13 | 4.14 |
| | | P30 | 2.28 | 8.77 | 3.09 | 0.81 | 1.55 | 0.91 |
| OA$^*$ | μg m$^{-3}$ | Max. | 5.48 | 11.31 | 6.88 | | | |
| | | P30 | 1.95 | 8.35 | 2.85 | | | |

OA$^*$: OA from VBS-HNOX simulations

**Table 4 Correlation coefficients between OA and $O_x$, SI-SOA and $O_x$, ASOA and $O_x$ and BSOA and $O_x$ for the flights on 16, 21 and 29 July, both from the measurements (AMS) and simulations with VBS-LNOX, VBS-HNOX and VBS-LA**

| Data | Date | OA/$O_x$ | SI-SOA/$O_x$ | ASOA/$O_x$ | BSOA/$O_x$ |
|---|---|---|---|---|---|
| AMS | 16$^{th}$ | 0.70 | | | |
| | 21$^{st}$ | 0.71 | | | |
| | 29$^{th}$ | 0.72 | | | |
| VBS-LNOX | 16$^{th}$ | 0.95 | 0.91 | 0.96 | 0.57 |
| | 21$^{st}$ | 0.95 | 0.77 | 0.85 | 0.90 |
| | 29$^{th}$ | 0.98 | 0.79 | 0.93 | 0.84 |
| VBS-HNOX | 16$^{th}$ | 0.96 | 0.90 | 0.96 | 0.45 |
| | 21$^{st}$ | 0.95 | 0.77 | 0.92 | 0.88 |
| | 29$^{th}$ | 0.98 | 0.78 | 0.95 | 0.80 |
| VBS-LA | 16$^{th}$ | 0.87 | 0.88 | 0.89 | 0.89 |
| | 21$^{st}$ | 0.67 | 0.83 | 0.68 | 0.65 |
| | 29$^{th}$ | 0.88 | 0.86 | 0.88 | 0.94 |

943 **Table 5 Slopes of OA vs. Ox, SI-SOA vs. $O_x$, ASOA vs. $O_x$ and BSOA vs. $O_x$ for the flights on 16,**
944 **21 and 29 July, both from the measurements (AMS) and simulations with VBS-LNOX, VBS-**
945 **HNOX and VBS-LA**
946

| Data | Date | $OA/O_x$ | $SI\text{-}SOA/O_x$ | $ASOA/O_x$ | $BSOA/O_x$ |
|---|---|---|---|---|---|
| AMS | 16th | 0.13 | | | |
| | 21st | 0.14 | | | |
| | 29th | 0.15 | | | |
| VBS-LNOX | 16th | 0.23 | 0.04 | 0.18 | 0.02 |
| | 21st | 0.29 | 0.02 | 0.11 | 0.16 |
| | 29th | 0.26 | 0.03 | 0.14 | 0.09 |
| VBS-HNOX | 16th | 0.15 | 0.04 | 0.10 | 0.01 |
| | 21st | 0.24 | 0.02 | 0.08 | 0.15 |
| | 29th | 0.19 | 0.03 | 0.09 | 0.08 |
| VBS-LA | 16th | 0.19 | 0.15 | 0.01 | 0.02 |
| | 21st | 0.07 | 0.03 | 0.00 | 0.03 |
| | 29th | 0.11 | 0.07 | 0.01 | 0.03 |

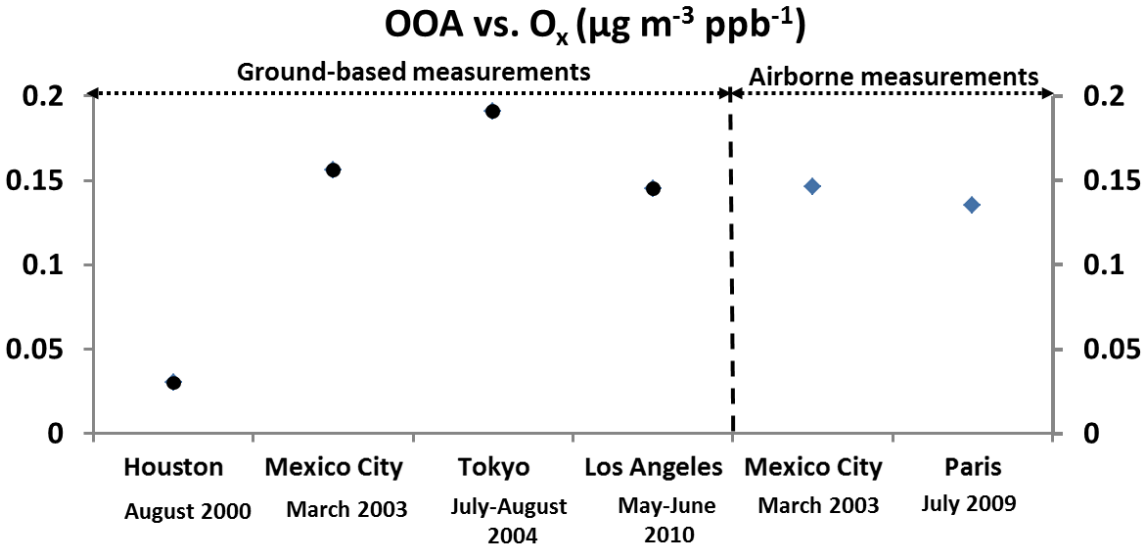


947

948 Fig. 1. Ratios of OOA vs. $O_x$ from studies in Mexico City, Houston, Los Angeles, Tokyo and Paris.
949 Ratios for Houston, Los Angeles and Tokyo are derived from ground-based measurements during
950 typically one month and located in the metropolitan area. For Houston, the ratio during influences
951 from a combination of urban and petrochemical emissions, typically 0.03 µg $m^{-3}$ $ppb^{-1}$ (Wood et al.,
952 2010), is presented. Ratios for Paris and Mexico City are derived from three and two individual flights,
953 respectively, performed at about 100 to 150 km downwind from the agglomeration.

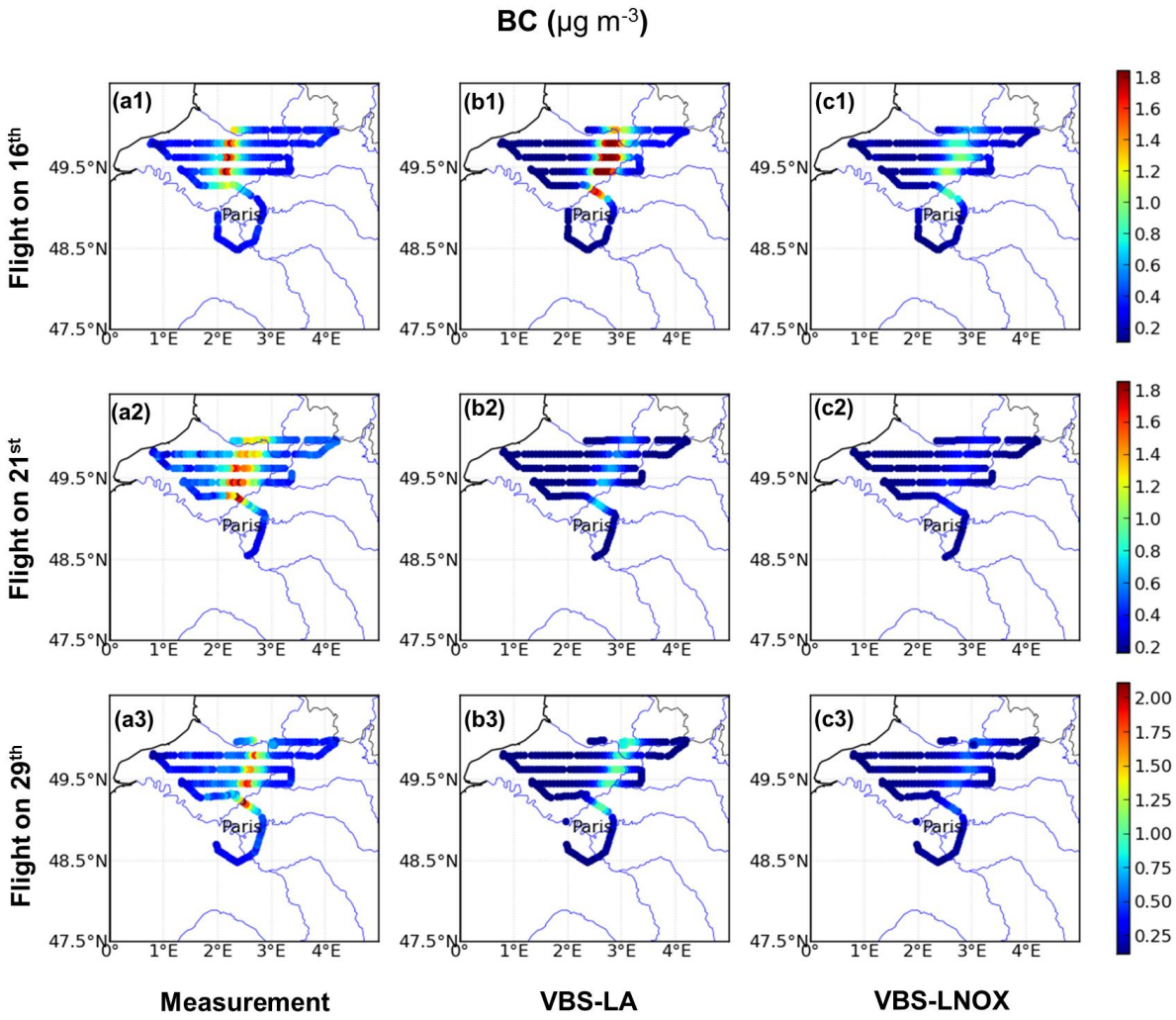


954

955 Fig. 2. Comparison of measured (a1, a2, a3) and modeled BC from VBS-LA (b1, b2, b3) and VBS-
956 LNOX (c1, c2, c3) during the flights on 16th, 21st and 29th, respectively.

957

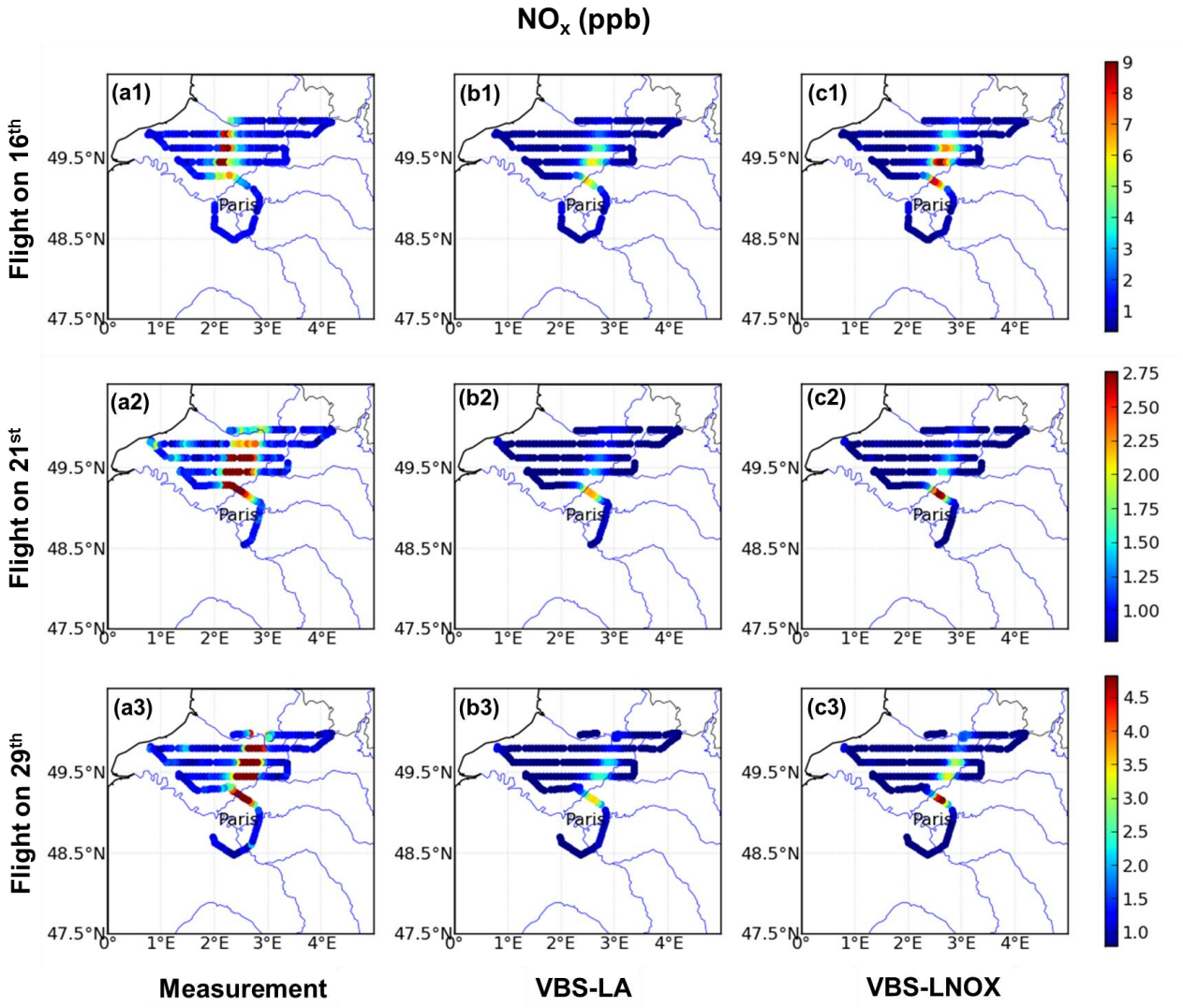


958

959 Fig. 3. Comparison of measured (a1, a2, a3) and modeled $NO_x$ from VBS-LA (b1, b2, b3) and VBS-
960 LNOX (c1, c2, c3) during the flights on 16th, 21st and 29th, respectively.

961

962

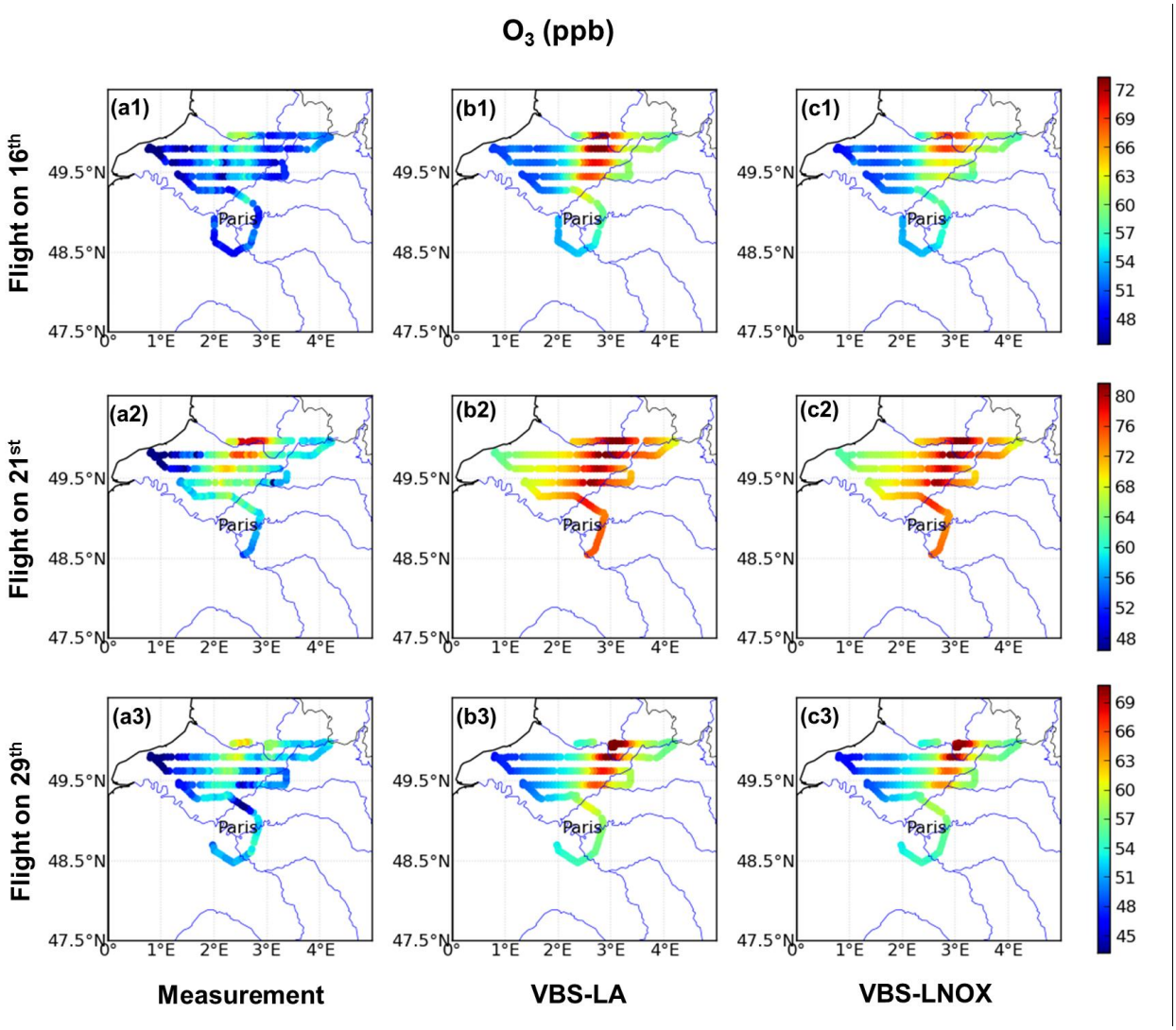


963

964 Fig. 4. Comparison of measured (a1, a2, a3) and modeled $O_3$ from VBS-LA (b1, b2, b3) and VBS-
965 LNOX (c1, c2, c3) during the flights on 16th, 21st and 29th, respectively.

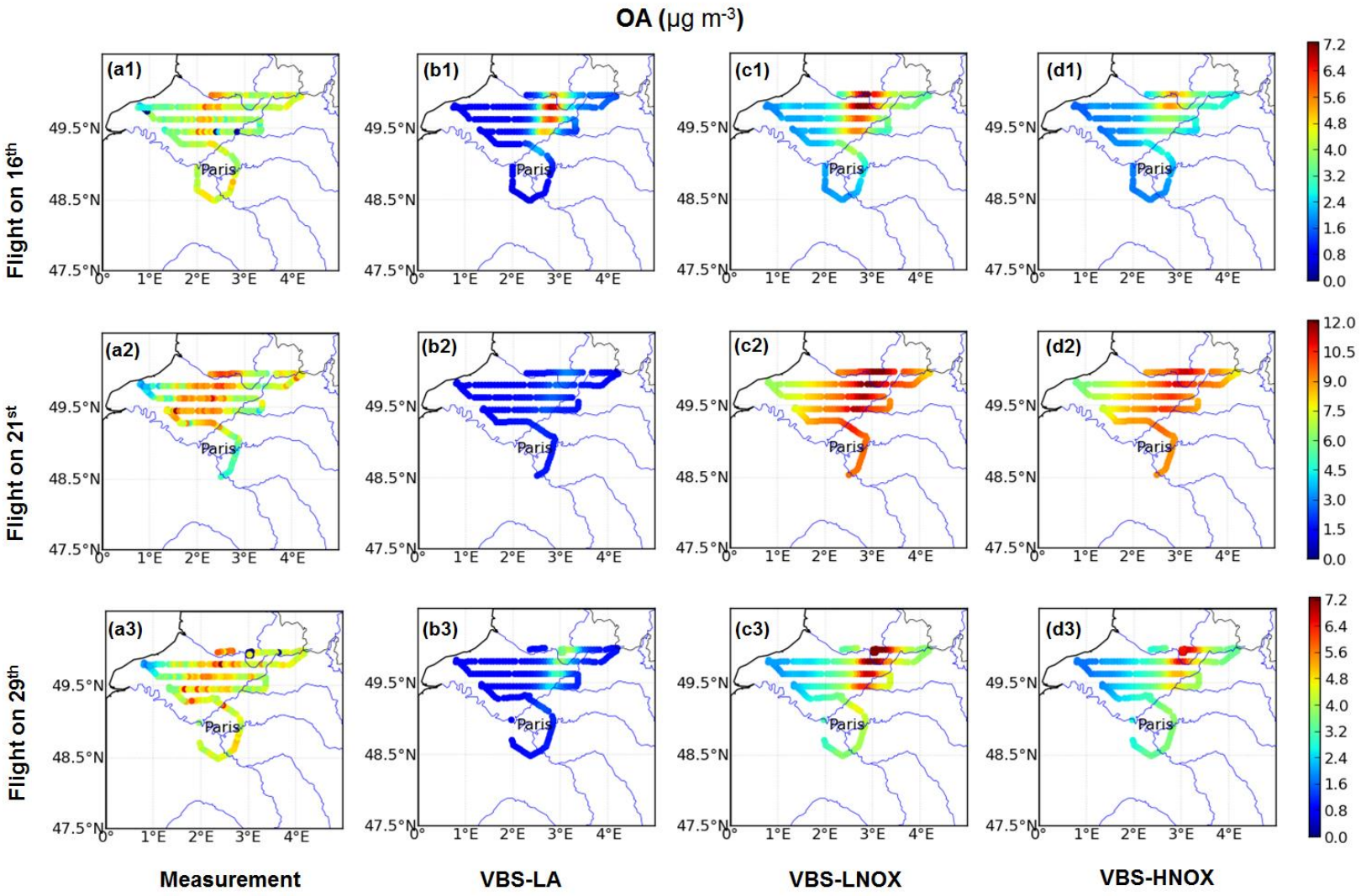


Fig. 5. Comparison of measured (a1, a2, a3) and modeled OA from VBS-LA (b1, b2, b3), VBS-LNOX (c1, c2, c3) and VBS-HNOX (d1, d2, d3) during the flights on 16th, 21st and 29th, respectively.

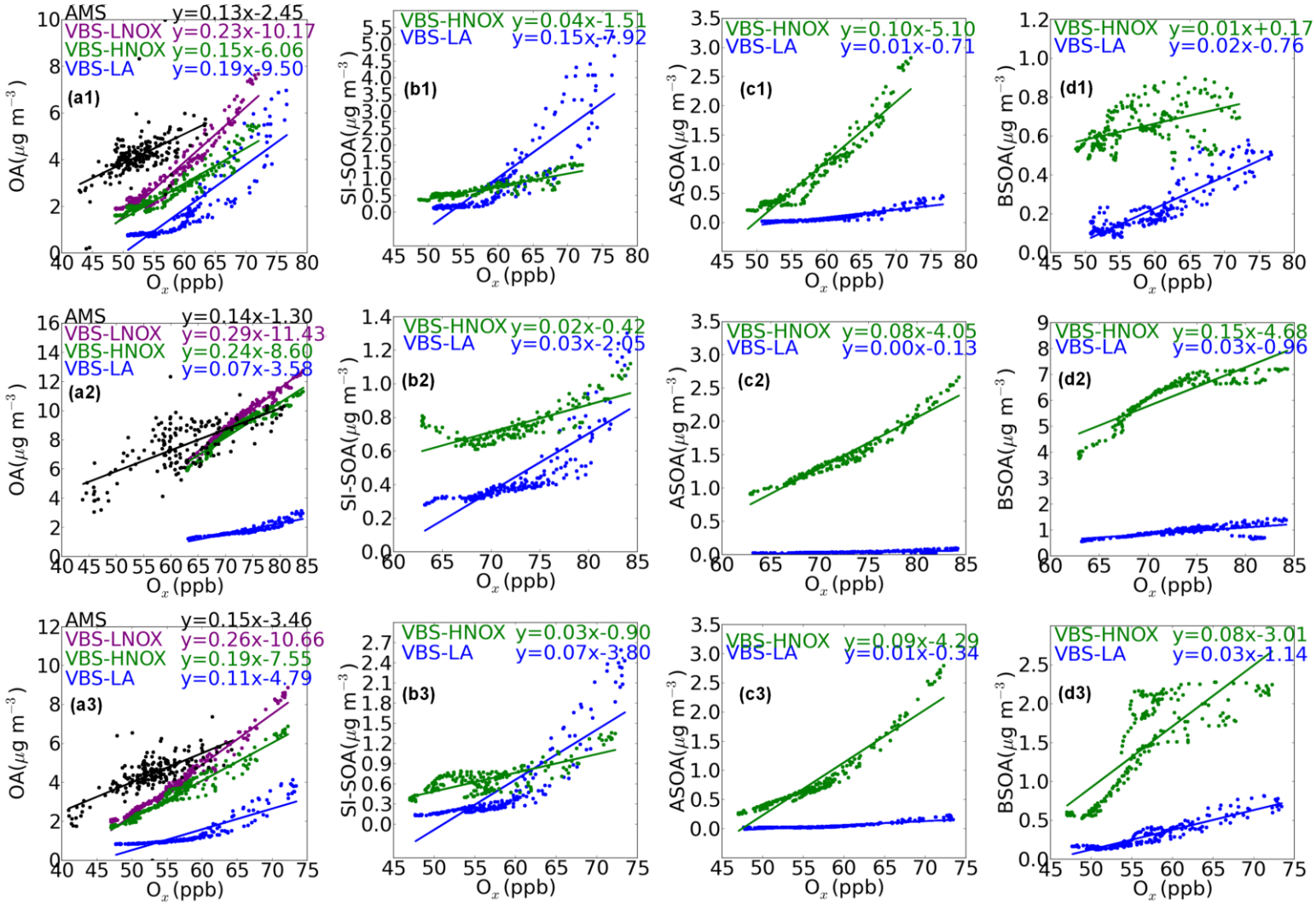


Fig. 6. OA vs. $O_x$ (a1, a2, a3), SI-SOA vs. $O_x$ (b1, b2, b3), ASOA vs. $O_x$ (c1, c2, c3) and BSOA (d1, d2, d3) vs. $O_x$ during the flights on 16$^{th}$, 21$^{st}$ and 29$^{th}$, respectively. For OA vs. $O_x$ (a1, a2, a3), results from the measurement, VBS-LA, VBS-LNOX and VBS-HNOX are presented. For others, only results from VBS-LA and VBS-HNOX are presented.

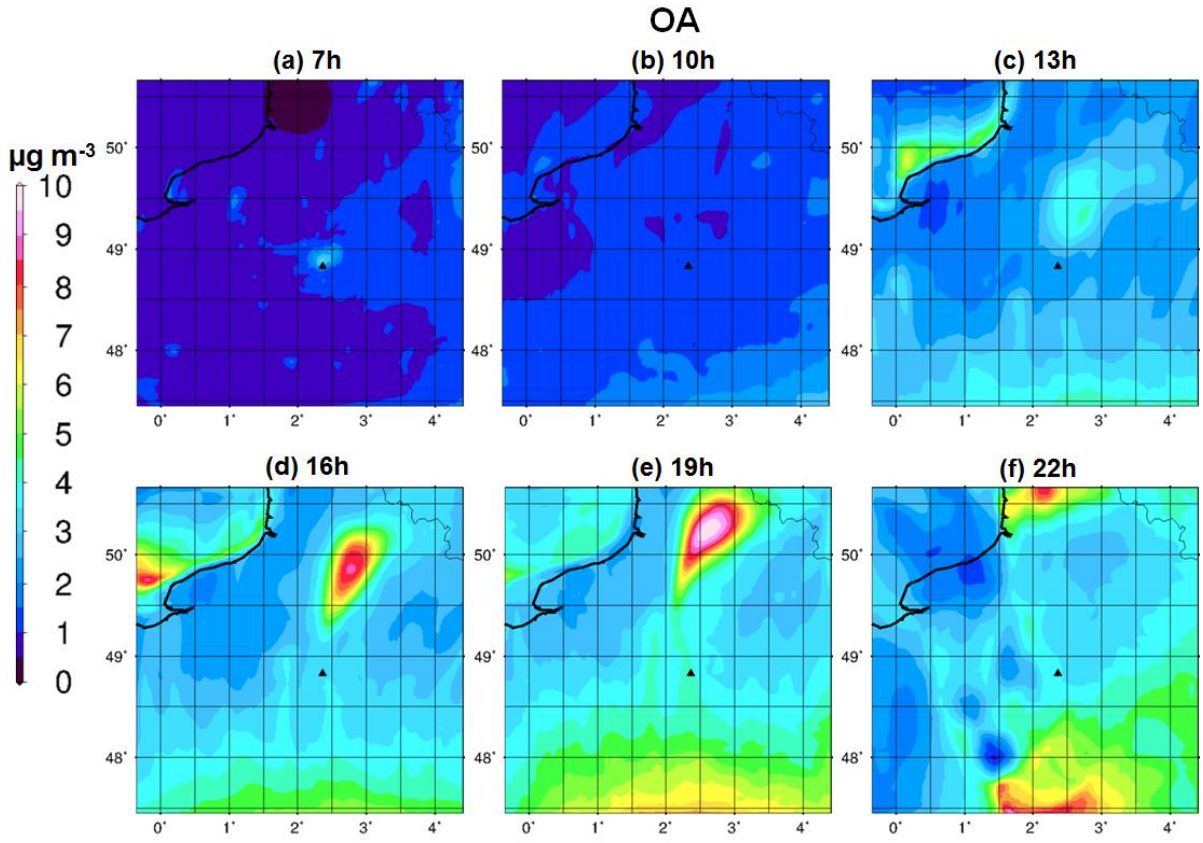


974

975 Fig. 7. Urban OA ($PM_{10}$ fraction) plume (µg $m^{-3}$) evolution on July 16$^{th}$ from VBS-HNOX, the
976 triangle represents the location of Paris, illustrated by 6 panels (from a to f) corresponding to 7h (UTC
977 +2) to 22h (UTC +2) with a time step of three hours.

978

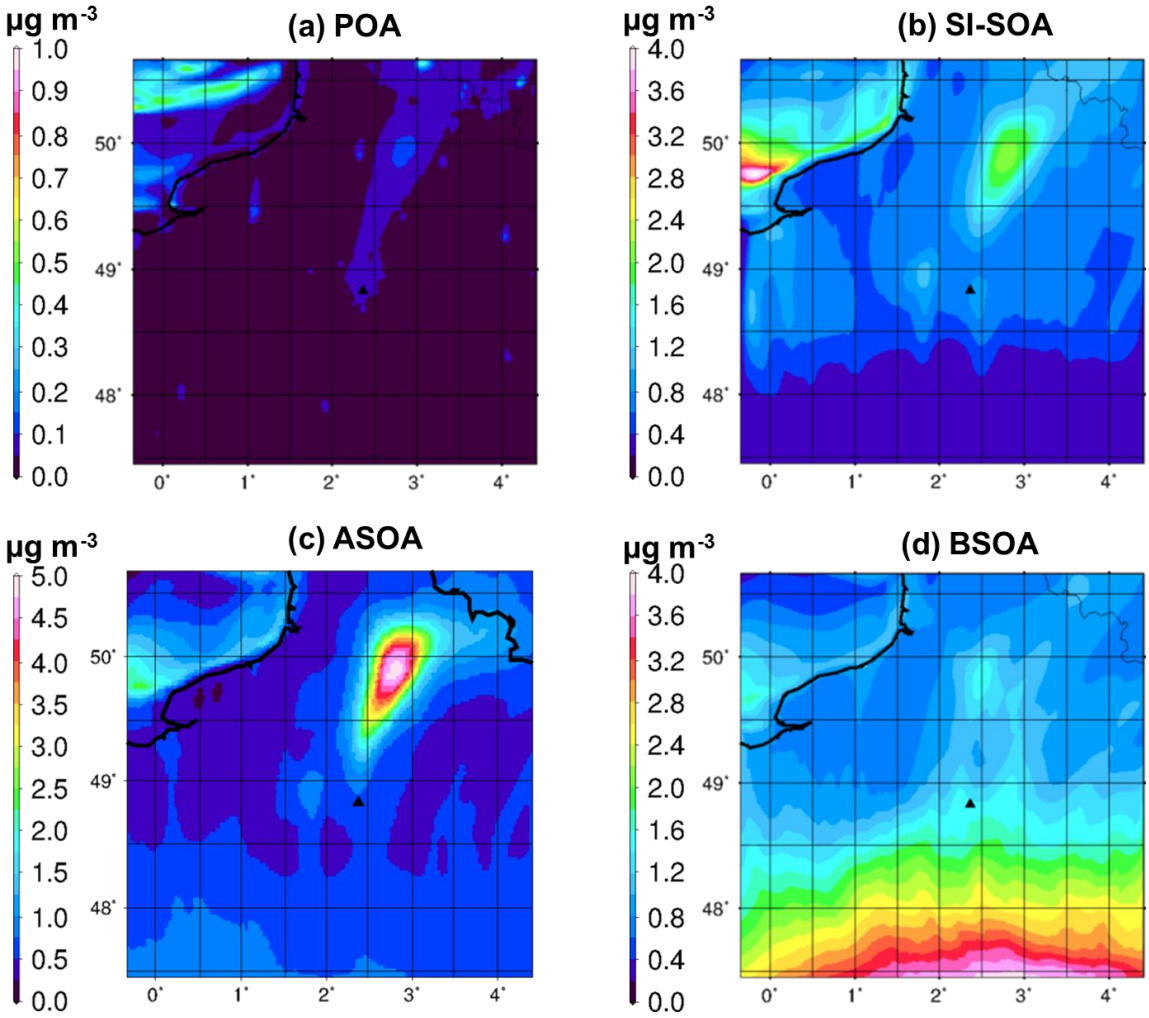


979

980 Fig. 8. Urban POA (a), SI-SOA (b), ASOA (c) and BSOA (d) (in $PM_{10}$) plume (µg $m^{-3}$) from VBS-
981 HNOX at 16h (UTC +2) of July 16$^{th}$ , the triangle represents the location of Paris.

982

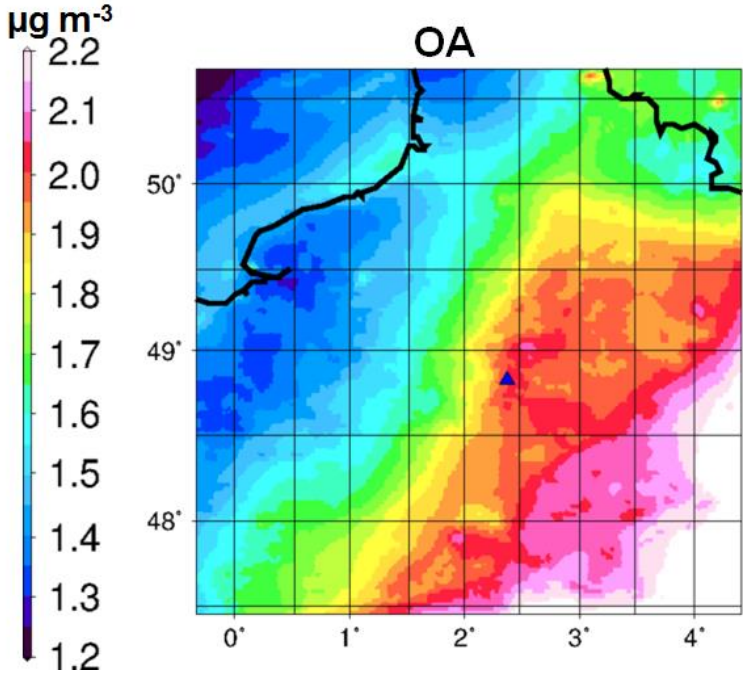


983

984 Fig. 9. Modeled monthly mean OA concentration in $PM_{10}$ (µg $m^{-3}$) from VBS-HNOX which
985 represents the influence of Paris emissions on OA levels, the triangle represents the location of Paris.

986

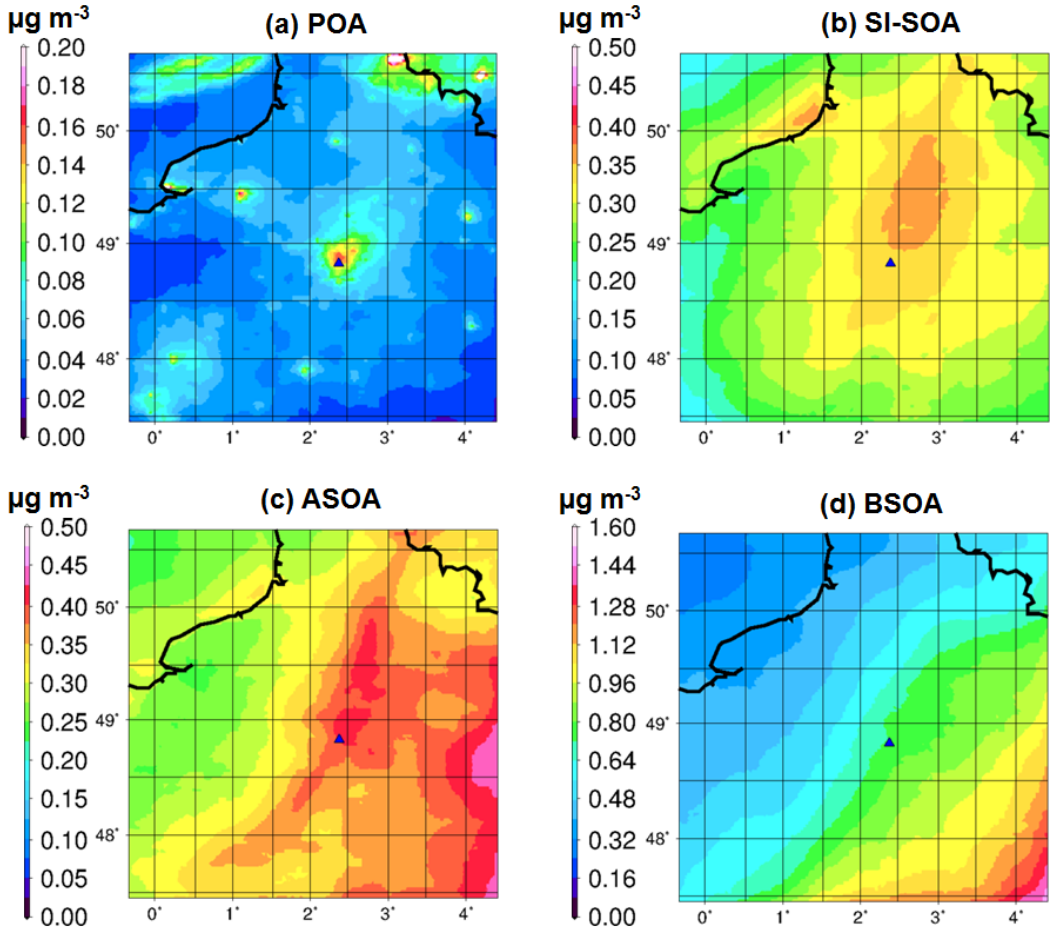


987

988 Fig. 10. Modeled monthly mean POA (a), SI-SOA (b), ASOA (c) and BSOA (d) concentration in
989 $PM_{10}$ (µg $m^{-3}$) from VBS-HNOX which represents the influence of Paris emissions on OA levels, the
990 triangle represents the location of Paris.